2015

Tracing Sediment in the Subsurface Using Beryllium-7: Green River Basin, KY

Caroline Adams Broderick
Louisiana State University and Agricultural and Mechanical College

TRACING SEDIMENT IN THE SUBSURFACE USING BERYLLIUM-7: GREEN RIVER BASIN, KY

A Thesis

Submitted to the Graduate Faculty of the
Louisiana State University and
Agricultural and Mechanical College
in partial fulfillment of the
requirements for the degree of
Master of Science

in

The Department of Geology and Geophysics

by
Caroline Adams Broderick
B.S. College of Charleston, 2011
May 2016

ACKNOWLEDGEMENTS

I would like to thank my major advisor, Dr. Carol Wicks, for her support and guidance on this project and my graduate school career. I would also like to thank Dr. Sam Bentley for field and laboratory work guidance. And I am very thankful for help from Dr. Jeffrey Hanor, on this project or any other I have had, who always had the time. I am also in debt to for fieldwork and brainstorming to Randall Paylor. Paylors' work focuses on understanding bedload transportation through karst, carbonate removal and effects on the global carbon cycle; where as this work investigates suspended and fine grained particles, together to quantify mechanical removal of carbonate in karst terrain for models of landscape denudation in carbonate basins. I would like to thank our funding from the National Science Foundation and my additional funding from the American Petroleum Institute. I would also like to thank those from the Kentucky Speleological Survey, who gave me access to invaluable data and maps for the successful completion of this project. Also many thanks to those peers that helped me with my laboratory work, Crawford White, Greg Keller, Jeff Bomer and Kathryn Dennomee.

Thank you to all my friends in graduate school that have given me inspiration to keep working and finish this project: Marie Thomas, Laura Sorey, Alesha Morabito, John Michael Callen and Derek Goff. Lastly I would like to thank my parents for hosting any graduate students that ever needed help along the way and my siblings: Peter, Olivia, and Philip.

TABLE OF CONTENTS

LIST OF TABLES

LIST OF FIGURES

ABSTRACT

As water flows through areas of limestone, karst inevitably develops, creating sinking streams and sinkholes that transport alumino-silicate particles from the surface into the subsurface. Sediment budget studies on short term scales through karst are rare. Thus, a feasibility study using beryllium-7 (^{7}Be), which attaches to soil particles and can be used as a short-term (2-3 month) tracer of the movement of fine-grained sediment in karst was investigated. Sediment samples were collected from a karstic catchment within Green River basin, Kentucky, both on the surface and in the subsurface along a cave stream. Samples were collected prior to and immediately after a recharge event that transported sediment into the subsurface. The before event samples were analyzed for the activity of ^{7}Be to establish a baseline activity for the isotope. The after event samples were collected from the same locations as the pre-event samples were collected and analyzed for ^{7}Be activity.

Average ^{7}Be activities measured after the recharge event were as predicted higher than measured ^{7}Be activities before recharge. Our findings indicate that radioisotope ^{7}Be is a viable tracer for sediment dynamics through karst on short-term time scales. Results demonstrate no strong correlation exists between sediment characteristics and ^{7}Be activity, but correspond to the general increasing trending of mean ^{7}Be activity with increasing average grain size and carbonate composition after recharge.

This research is important to understanding sediment movement from the Earth's surface into the subsurface and subsurface sediment dynamics. The potential applications of further studies of ^{7}Be in karst systems and rapid underground sediment dynamics are multi-variable. Future ^{7}Be studies can be applied to trace contaminants as they move through karst systems, to

quantify source to sink sediment budget systems, to understand global carbon cycle sinking mechanisms.

CHAPTER I. INTRODUCTION

To quantify the rapid (2-3 month) movement of fine-grained sediment through karstic basins, it is necessary to understand the process of sediment movement in the subsurface over short time scales due to the uniquely rapid nature of fluid movement through the conduits of karst systems. (e.g. White, 1989; Mahler *et al.*, 1998; Dogwiler and Wicks, 2004; Lynch *et al.*, 2004; Bosch and White, 2007; Gentry, unpublished). Many karstic basins are susceptible to large short-term hydrologic variations. As the basins fill and empty so rapidly, a sediment tracer with a comparable residence time is needed (Long and Mahler, 2013). To understand these dynamics, studies have proven that virtually all sediment transport through karst systems occurs during or immediately following storm events (e.g., Mahler and Lynch, 1999). According to Mahler *et al.* (1998) the best way to calculate the residence times of sediment in karstic basins is through the use of particle tracing.

This study introduces a new method of particle tracing using radioisotope beryllium-7 (^{7}Be) to calculate short-term residence times of sediment in karst surrounding a recharge event. I predict that activity of radioisotope ^{7}Be found in sediment in a karstic basin before a recharge is less than the activity of ^{7}Be after a recharge event. To verify the results of this study, mineralogic and grain size analyses were conducted on a representative number of collected samples to determine if a relationship exists between ^{7}Be activity and the sediment characteristics. The process (mechanical abrasion) of physical as opposed to chemical weathering (dissolution) is one purpose for investigating the use of a ^{7}Be particle tracer in this research and this work will aid in the detailed accounting of mechanical abrasion associated with karst regions. This new method could be integrated into the geochemical models of karst landscape denudation currently available (Palmer).

The rates and preferred pathways of sediment transport in many karst systems can be considered unquantifiable at present due to the limitations of sediment tracers currently in use (e.g., Mahler *et al.*, 1998; Walling, 2013). Most attention has been given to subsurface water tracing, but the first studies that experimented with tracing sediment particles through karst used *Lycopodium* spores dyed several different colors (Drew and Smith, 1969; Aley and Fletcher, 1976; Atkinson *et al.*, 1973). Mahler *et al.* (1998) used lanthanide ion tracers to map clay movement through a karstic basin. These tracers worked on time scales of minutes to hours and are thus incapable of measuring sediment movement through karst systems over weeks to months.

There are several reasons to quantify sediment transport through karstic basins, including mapping contamination pathways, understanding sediment budgets, and investigating changes to cave stream geomorphology. The most important reason is to understand contaminant pathways. One study demonstrated that suspended sediment transport is the controlling mechanism of environmental contaminants in karstic basins (Loop and White, 2001). In addition to understanding contaminant movement through karst, quantifying sediment transport can also illustrate changes to sediment budgets, which are strong indicators of changes in a basin (Blake *et al.*, 2002). Dogwiler and Wicks (2004) showed that sediment movement through karstic basins during high discharge events could rapidly change the geomorphology of cave streams.

Several different methodologies have been employed to understand subsurface sediment movement. Mahler and Lynch (1999) collected hourly samples of suspended sediment during a storm event, then used mineralogical and grain size analyses to quantify sediment movement through karst and showed that seasonal effects on surface sediment supply may be important due to the quantity of sediment moving and its potential to carry contaminants. Lynch *et al.* (2004)

used mineralogical analysis to quantify suspended sediment characteristics to determine the origin of the sediments moving through karstic basins and to find the rate and distance of potential contaminant movement. Other investigations have also used $^{26}Al/^{10}Be$ isotopes in karst to better understand cave development on million year scales (Stock *et al.* 2005).

Sediment transport through karstic basins has previously been investigated using radioisotopes cesium-137 (^{137}Cs) and lead-210 (^{210}Pb) on yearly rates to address problems in sediment supply, transport, and deposition (e.g., Murray *et al.*, 1993). Many studies have investigated sediment movement and dynamics through karstic basins, although no research prior to the study reported here has investigated the use of radioisotope ^{7}Be as a short-term tracer of sediment movement in karst. This necessitates a feasibility study for using ^{7}Be as a short-term tracer of sediment movement in karstic basins. This can be tested by analyzing samples before and after recharge events. The naturally occurring radioisotope ^{7}Be has a short (~53.3 days) half-life and is ideal for tracing the mechanical movement of particles through karst systems over an estimated ~3-5 month time frame (Rotondo and Bentley, 2003). For this study, I chose the Hidden River Cave as a study site. This is part of Mammoth Cave System and is located in Kentucky.

CHAPTER II. BACKGROUND

2.1 Geologic Setting

2.1.1 Karst Geology

Karst is a landform that represents the geologic phase of a carbonate basin, usually limestone, between deposition and complete erosion that develops when the rock comes into contact with slightly acidic rainwater (Livesay and McGrain, 1962; Palmer, 2012). Karst is marked by sinkholes that form through chemical (dissolution) and mechanical abrasion by water through streams, fractures or seepage that eventually become large enough to form caves (Figure 1). Caves are sensitive to changes in landscape and water flow because their development is connected to river incision and sediment accumulation (White, 1988; Granger and Fabel, 2012). Chemical weathering occurs when rainwater combines with atmospheric carbon dioxide to form carbonic acid. The slightly acidic precipitation comes into contact with the calcium carbonate of limestone. The calcium carbonate in limestone reacts with the carbonic acid to form calcium bicarbonate, which is a soluble compound that is dissolved into water (White, 1989). Carbon dioxide is the only gas that can dissolve carbonates in this environment.

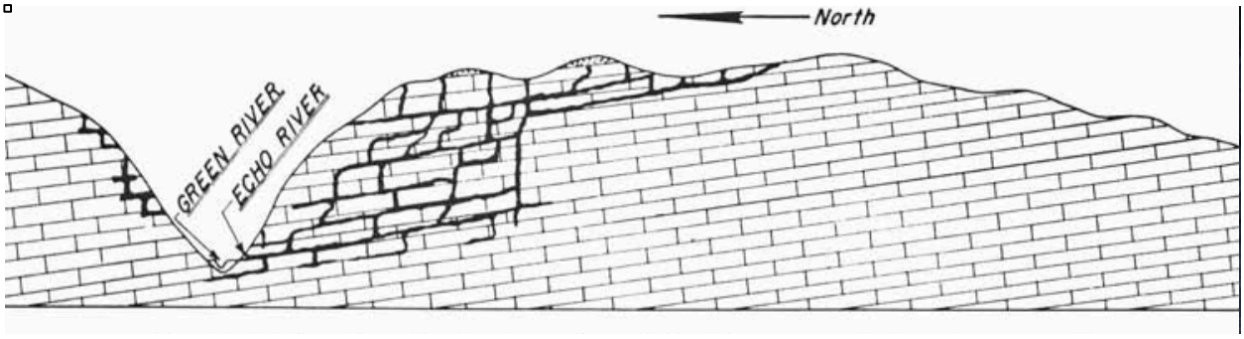

Figure 1. Schematic diagram of karst development in the Mammoth Cave area with the Green River as base level (Livesay and McGrain, 1962).

2.1.2 Geology of Mammoth Cave, Kentucky

The limestone units of the Mammoth Cave area are of Mississippian age, and formed when the area was covered by a shallow sea and carbonate deposition occurred (Hess *et al*., 1989; Palmer, 1991). A drop in sea level along with a mass marine extinction marked the end of the Mississippian period. During this time new mountain building was occurring in North America due to Gondwana colliding into Lauruasia to form the supercontinent Pangea, which formed the Appalachian. After the end of the Paleozoic, the Mammoth cave area was uplifted on the margin of the Cincinnati Arch (Figure 2) and has subsequently underwent erosion since that time shaping the present landscape.

The Mammoth Cave area limestone formations began developing karst during the Oligocene Epoch (30-25 Ma) when erosive processes began to dominate (Livesay and McGrain, 1962; May *et al*., unpublished guide). The formations that make up the karst topography are in Illinois, Indiana, Missouri, and Kentucky (Russell, 1932; White, 1989). Mammoth Cave exists within four formations in stratigraphic order from oldest to youngest, the St. Louis Limestone, the Ste. Genevieve Limestone, the Girkin Limestone and the Big Clifty Sandstone (Figure 3). The Appalachian Mountains are the ultimate sediment source for the Big Clifty sandstone, the youngest formation at Mammoth Cave (Thornberry-Ehrlich, 2011). The Big Clifty Sandstone rests on top of the limestone layers acting as a cap rock, which prevents complete failure of underlying layers. This stabilizes the slow degradation of limestone (Livesay and McGrain, 1962; May *et al*., unpublished guide). Uniform stratigraphy and deposition allow for use of the stratigraphic information from the well-studied Mammoth Cave (May *et al.*, unpublished guide).

The karst topography and base level for the Mammoth area developed contemporaneously with the slow downcutting of the Green River through the limestone units.

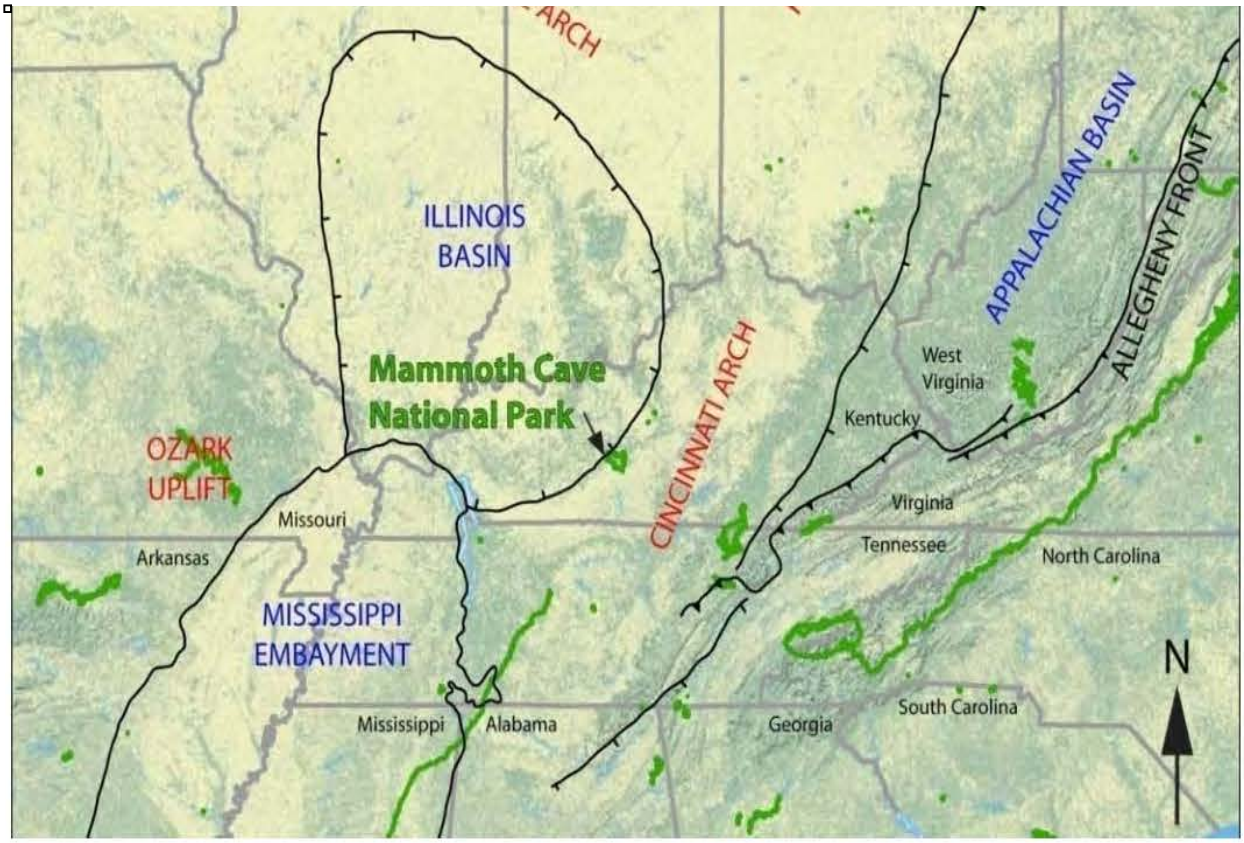

Figure 2. Geologic setting of Mammoth Cave Area, Kentucky. National Park Service units are in green including Mammoth Cave (Thornberry-Ehrlich, 2011).

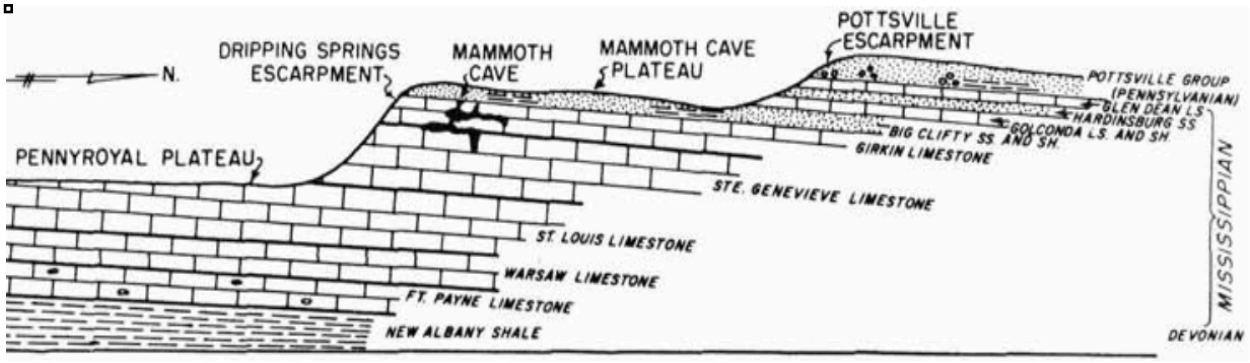

Figure 3. Cross section and stratigraphy of the Mammoth Cave Area (Livesay and McGrain, 1962).

This is controlled by groundwater flow that yields relatively horizontal openings during formation (May *et al*., unpublished guide; Thornberry-Ehrlich, 2011). The various levels of the cave system indicate that its development has happened over numerous pulses that are connected

to Cenozoic periods of glaciation in North American history (Granger and Fabel, 2012). Chemical weathering of limestone, operates below the Green River water table and works more slowly than the mechanical weathering processes that dominate above the river (Hess and White, 1989).

2.1.3 Hidden River Cave and the Green River

The Cincinnati Arch uplift in the eastern part of Kentucky caused direction of ground and surface water flow of the area to move westward and empty in the Green River. When rain falls on the Mammoth Cave Plateau (Figure 3) it seeps underground to the limestone layers and travels north both through underground and surface streams. Streams alternately sink and reemerge on the surface until they discharge into the westward flowing Green River. Dye tracing has confirmed water travels north from through Gorin Mill catchment, through Hidden River Cave and empties into the Green River (Hess *et al.*, 1989; Toomey and Olson, 2013). The Green River is one of the only continuous surface streams in the area and is the base level for karst development. The Green River empties into the Ohio River, which flows into the Mississippi and ultimately these sediments sink into the Gulf of Mexico.

There are two dominant sources for detrital sediment that accumulates in karst terrain. Firstly some allochthonous sediment such as sand, mud and silt may be brought into caves from the overlying soil or some further distance away. Secondly, some autochthonous sediments moving through the karst system could have originated from the limestone or sandstone layer above the cave passage (Livesay and McGrain, 1962). Regardless of source, the fine-grained sediment could be carried through the entire karst basin during a recharge event, could be carried into and depositied within the karst basin during a recharge event, or could be eroded from within the cave and carried farther downstream.

2.1.4 Hidden River Cave Study Site

The study site was the Gorin Mill sub-basin (Figure 4) and the subsurface karst systems known as Hidden River Cave. The study area is part of the Mammoth Cave, located about seven miles due east of the National Park perimeter. This site was selected due its accessibility for sampling. The surface samples (Table 1) were taken within the Gorin Mill sub-basin, a karst system with an area of approximately 900 km^2. The sediment sink of this study site is the Green River.

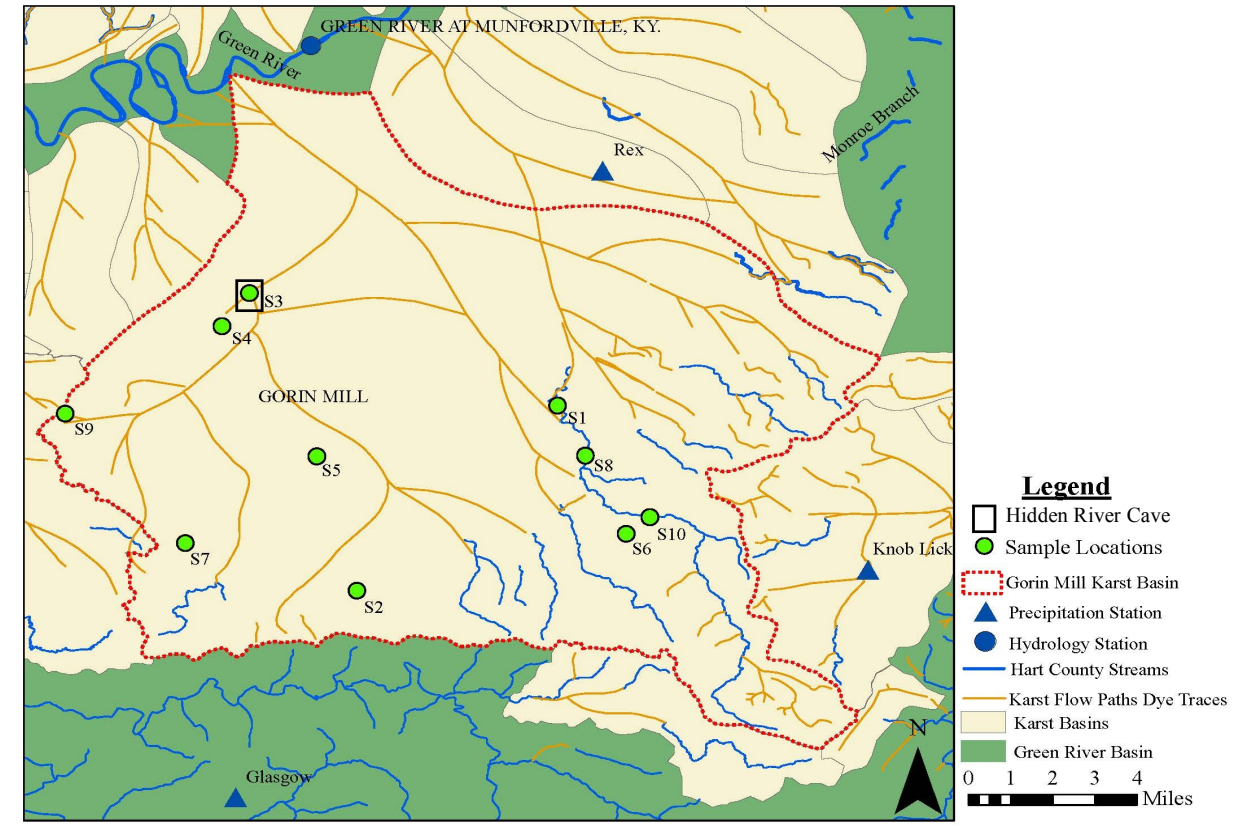

Figure 4. Gorin Mill karst catchment basin to the Green River with surface sample locations, Horse Cave is the surface equivalent of subsurface Hidden River Cave (GIS data from Kentucky Geological Society).

A map of Hidden River Cave (Figure 5) and the cave sampling locations (Table 2) show the subsurface sampling profile. The mouth opening at the entrance to Hidden River Cave formed when a sinkhole collapsed due to the instability of the underlying limestone layers

(Livesay and McGrain, 1962). This entrance to the cave is located in the middle of the town of Horse Cave, Kentucky.

Table 1. Surface Sample Locations and Map Identifications

Map ID	Environment	Sampling Trip	Samples Taken
S1	Tributary stream	Third	1
S2	Dry soil over LS bedrock in thin grassy area	Third	1
S3	Entrance to Hidden River Cave		0
S4	Corn Field	First and Third	6
S5	Waist-high grass on top of ridge	Third	1
S6	Sediment accumulation in bottom of sinkhole	Third	1
S7	A small eroded gully off of cornfield	Third	1
S8	Tributary stream	First	4
S9	Grassy Sinkhole	Third	1
S10	Tributary stream	First	4

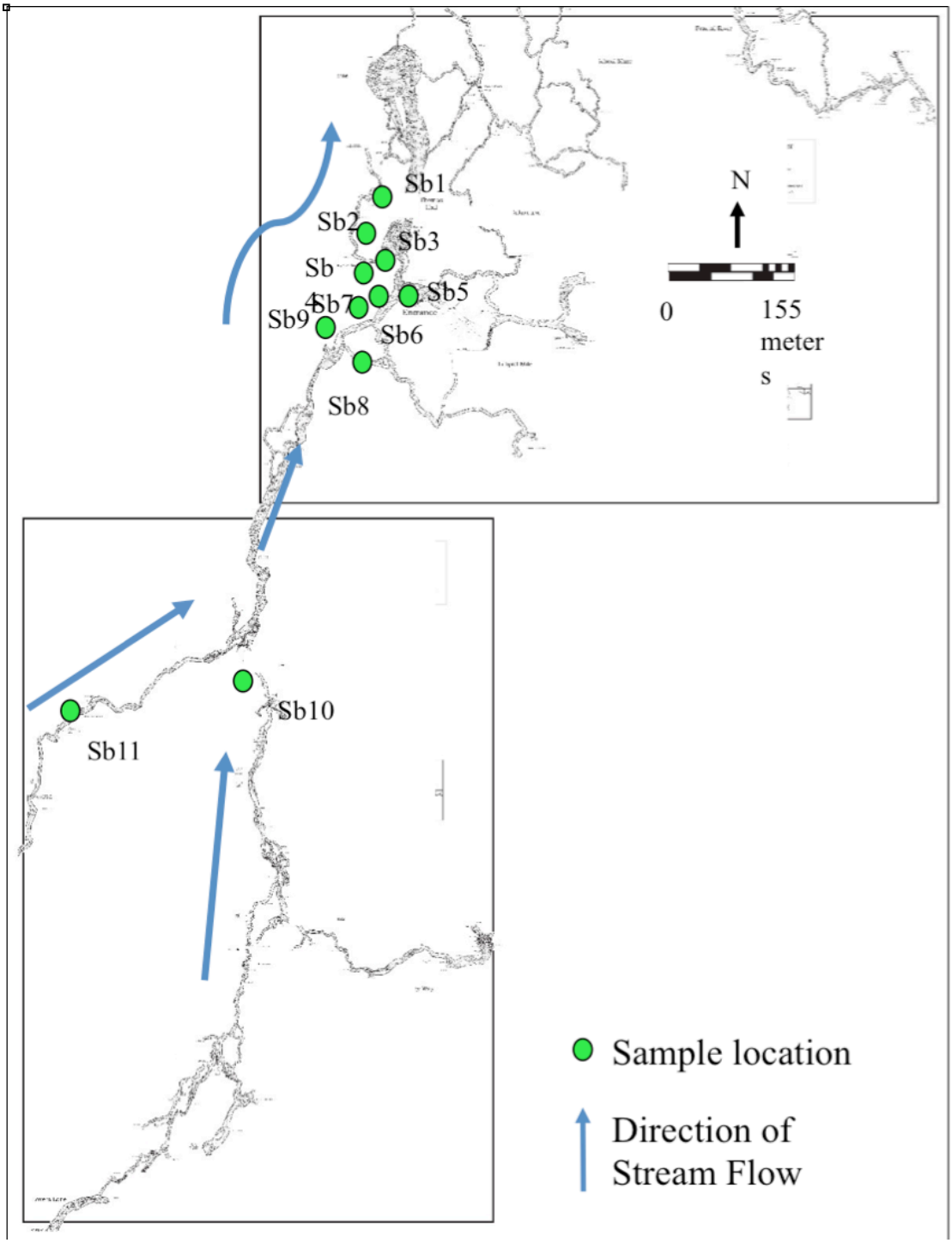

Figure 5. Partial map of Hidden River Cave located beneath the town of Horse Cave, Kentucky. Cave passages are black sinuous lines (Modified from West, 2013).

Table 2. Cave sample locations and map identification

Map ID	Environment	Sampling Trip(s)	Samples Taken
Sb1	Large sediment pile in a wide passage	Third	8
Sb2	First breakdown just below water line	Third	3
Sb3	Sediment bank next to walk way along the water	First and third	7
Sb4	Sediment drape on ledge next to walkway	Third	1
Sb5	High water mark from storm	Second	1
Sb6	Sediment deposit at bottom of stairs at receding flood	Second	1
Sb7	Cave City Spring at ledge 1.5' above stream water	Third	1
Sb8	Sediment bar at water level in a narrow passage	Third	1
Sb9	Left wall of South River looking upstream	Second and third	3
Sb10	Stream passage	Third	2
Sb11	Muddy deposit in small overflow passage pool at water level	Third	1

2.2 Beryllium-7 Isotope

This study makes use of isotopic dating using the natural radioisotope beryllium-7 ($t_{1/2}$=53.3 days). Extensively used isotopic tracers for sediment budget studies, cesium-137 ($t_{1/2}$ = 30.2 years) and lead-210 ($t_{1/2}$ = 22.2 years) do not account for short-term timescales (Blake *et al.*, 2002). ^{7}Be could be an ideal tracer, because it is a naturally occurring radioisotope with a short half-life needed to track short term sediment dynamics. The level of ^{7}Be activity in this study will yield the residence time of sediments within three to five half-lives (Rotondo and Bentley, 2003;Granger and Fabel, 2012).

^{7}Be forms from energetic particles that develop in the galaxy. These charged particles are composed of 90% protons and 10% alpha particles and travel across galactic space as primary cosmic rays. As these charged particles travel weak magnetic fields in the galaxy and on earth cause them to scatter and move in random directions (Brost *et al.*, 1991). The collision of

charged particles and atoms in the stratosphere, produces cosmic-ray secondary and tertiary particles, which are low energy neutrons (Junge, 1963). As these neutrons continue falling toward earth through the atmosphere they hit oxygen and nitrogen atoms, and these collisions produce a nuclear disintegration. A small part of these disintegrations produce ^{7}Be. Newly created ^{7}Be atoms then diffuse through the atmosphere until the atom hits a dust particle, usually between 0.03 and 1 micron (μ) in size, and the particles scavenge ^{7}Be. These submicron particles will then continue floating through the stratosphere or lower atmosphere where radioactive decay continues. About 59% of ^{7}Be atoms decay in the atmosphere; the other 41% of ^{7}Be atoms fall surface of the earth (Brost *et al.*, 1991). Of all the ^{7}Be that reach earth, 94% are through precipitation and only 6% are from dry deposition, the ^{7}Be adsorbs to the surface of sediment particles.

^{7}Be decays into lithium-7 through orbital electron capture (Walsh and Wellman, 2009). Orbital-electron is a type of decay by electron capture that arises for isotopes with surplus of protons in the nucleus and forms as the nucleus tries to become balanced with equal numbers of protons and neutrons. When a proton from the nucleus reacts with one of the electrons from its orbital, it transforms into a neutron and is described by Equation 1 below (Hans, 2001):

$$^{7}\mathrm{Be} + e_k \quad ^{7}\mathrm{Li} + \nu \qquad (1)$$

where e_k is an electron captured from the orbital K electron cloud surrounding the nucleus that reacts with a proton. This decay emits the daughter ^{7}Li and v which is a neutrino, a massless particle.

2.2.1 Previous Research using ^{7}Be

Previous studies have effectively used ^{7}Be in sediment budget research (e.g., Bonniwell *et al.*, 1999; Sommerfield *et al.*, 1999; Blake *et al.*, 2002; Rotondo and Bentley, 2003; Gentry,

unpublished). However, this research was conducted on surface processes. Early investigations of ^{7}Be as a tracer of dynamic processes, such as Brost *et al.* (1991), used the isotope to trace global climate and atmosphere dynamics models integrated in conjunction with lead 210 (^{210} Pb) data. Studies began using ^{7}Be to trace erosion rates and sediment dynamics in the late 1990s. A study by Sommerfield *et al.*,(1999) used ^{7}Be activities to trace sediment transport processes on the Eel River in Northern California proving its use for investigating flood sedimentation. Another study by Bonniwell *et al.* (1999) used ^{7}Be in tracing move out rates of suspended sediment in mountain streams. One study investigated the validity of using ^{7}Be in sediment budget research to find soil erosion and sediment movement and contaminant transfer, for specific recharge events (Blake *et al.*, 2002).

Sediment budget investigations have successfully used ^{7}Be as a tracer in fluvial environments and have shown that ^{7}Be was an excellent tracer of fast acting sedimentary agents like river discharge and waves (e.g. Rotondo and Bentley, 2003; Corbett *et al.*, 2007). Recent studies have used ^{7}Be coupled with ^{137}Cs and ^{210}Pb for investigation of land degradation and sediment residence times in catchment systems (Evrard, *et al.*, 2010). Bentley *et al.* (2014) integrated all three environmental tracers to investigate deposition and bioturbation of terrestrial to marine sediments.

While the above studies prove the validity and utility of ^{7}Be, all of this research was conducted on surface processes. Due to short duration and high intensity recharge events that dominate karstic basins, it is necessary to understand frequency and magnitude of recharge and subsequent effects (Groves and Meiman, 2005). An investigation of ^{7}Be in karst systems is presented here to quantify contaminant transport, source to sink sediment budgets and event-based geomorphology responses through the surface to subsurface.

CHAPTER III. SAMPLING AND TECHNIQUES

3.1 Field Methods

The study site, Hidden River Cave and Gorin Mill catchment system (Figures 4-5) is located in west central Kentucky and was selected to conduct this study because of accessibility. Hidden River Cave is a part of the well-known Mammoth Cave System, but not located within the National Park boundary as the Park does not include the entire cave system.

Fifty two sediment samples were collected in April and May of 2014 (Tables 1-2). These dates were selected to capture data from the peak spring rainfall events with the assumption that the largest annual rainfall period would have the highest discharges of the year and move the largest volume of sediment. Precipitation and discharge data were obtained and integrated into this research (Figures 8-9).

The catchment area, surface streams, karst conduit pathways, the Green River, hydrologic collection sites and surface sample locations are shown in Figure 5. The catchment system (sub-basin) area of this study is approximately 900 km^2. No precipitation measuring station was located in the sub-basin, so the precipitation and discharge data were obtained and subsequently averaged from the United States Geological Survey data Munfordville monitoring station at the Green River, the National Oceanic and Atmosphere Administration (NOAA) monitoring stations at Knob Lick and Rex, and from the Glasgow Airport.

Samples collected in April 2014 act as background samples for this research and were collected as sediment cores from surface streams and locations around the surface of Gorin Mill basin and subsurface of Hidden River Cave. Samples were collected from the first trip on April 15-16th, 2014 (Figure 6) and during storm event samples April 29th-May 1st, 2014 (Figure 7). On the third trip samples were collected May 20th and 21st after spring storm events and represent

Figure 6. Entrance of Hidden River Cave and stream before recharge event on 4/15/14 (photo by Randall Paylor, unpublished).

Figure 7. Flooded entrance to Hidden River Cave during recharge event on 5/1/14 (Photo by Randall Paylor, unpublished).

the response of suspended load. The entrance is marked on the surface map as sample locations S3 and on the subsurface map, sample location Sb5 marks a sample taken at the high water mark of sediment deposition on the stairs after the storm that occurred in the study area on April 29-30th, 2014.

The direction of stream flow in the cave is to the north and samples Sb11 and Sb10 were the most upstream subsurface samples and samples from the Sb1 passage were at the most downstream sample location. The stream channel in the most upstream passages at the Sb10 and Sb11 locations was roughly a meter to a meter and a half wide, with a depth of ten to fifteen centimeters. The stream channel in these passages did not reach from bank to bank. The sides of passages showed evidence that the passage had been filled to various levels previously as mud was draped up to the sides around a meter up from base level. This is also evidence that water periodically will rise to completely fill cave passages.

Further downstream at sample location Sb9, the stream channel was slightly deeper, and while still incised the channel did not reach the edges of the passages or the stream banks. The cave passage at Sb8 was roughly a meter vertically and horizontally a meter or slightly wider. This passage was much narrower than other sampled passages and researchers were required to crawl on hands and knees through ten centimeter depth slow moving water after recharge event. The stream channel to reach sample location Sb8 was deeply incised into the cave floor. Downstream into the passage around Sb7 and Sb4, the stream flow widened to reach each bank and deepened to approximately a third to a half meter. The furthest downstream passages sampled were ten meter vertically and roughly ten meters wide in the Sb1 and Sb2 locations. Both of these sediment banks were eight to nine meters high. The stream moved fastest here and curved around the large sediment piles where samples were collected.

Subsurface sampling locations are show in Figure 5 and associated data in Table 2. On the first sampling trip, sediment sampling in the cave consisted of a single downhole core located at a sediment bank along the subsurface stream near to the entrance at Sb3. This core was taken from the surface to twenty five centimeters using a hand auger and split into six samples during collection. On the second trip a sample Sb5 was taken from the highest water mark caused by the storm event, and samples were taken at Sb2, Sb6 and Sb9 as storm waters receded and the water levels lowered enough to allow researchers to enter the cave (Figure 8). These samples were all collected from zero to one centimeter depth.

Samples collected after the recharge event were taken upstream (Sb7-11) and downstream (Sb1-Sb4) of the entrance to the cave. A sample was taken at the sediment bank at Sb3, the same location as the before recharge event cave sediment core. Sample location Sb1 is a large sediment pile in a wide passage where a cross section of samples was taken.

At the very top of the Sb1 location, samples were taken from zero to three centimeters at one centimeter intervals. Other samples taken downstream of the entrance were Sb2 and Sb4. Sampling at Sb7 through Sb11 was upstream of the entrance. The sediment samples from the Sb10 cave passage were from stream level and the second one along a ledge 1.2 m directly above water level.

Sampling covered a range of topography from streams, sinkholes and fields to understand which areas would have the most ^{7}Be activity and the most recent sediment movement. Surface samples were taken at various locations around the Gorin Mill sub basin are described in Table 1. Sampling specifically targeted the western section of the basin that would feed into Hidden River Cave (Figure 4). Samples were taken along tributary streams and in fields farther away from tributary streams. The basin is marked with sinkholes, some with and others without the

without standing water and these areas were also targeted for surface sampling. Surface sample location S4 was a fallow cornfield and the closest sample location to the entrance of the cave.

Sediment cores from the first trip ranged between zero to twenty five centimeters, on the second and third trips shallower samples were collected from subaerial locations around the surface and subsurface of the basin before, during and after storm events. Sampling from second and third trips was conducted at zero to one centimeter intervals, with the exception of one to three centimeters at the H6 level of Sb1. This depth in sampling was due to the assumed low activity of ^{7}Be at depths greater than a few millimeters (Mabit *et al.*, 2008).

Samples were brought back to Louisiana State University Geology and Geophysics Department and all testing for ^{7}Be activity, grain size and mineralogy was completed.

3.2 Laboratory Methods

I processed samples in a gamma spectrometer. Measured ^{7}Be counts allow us to calculate activity at collection time as dpm/g (the number of atoms that have decayed in one minute per gram) for that region of the isotope spectrum (Corbett *et al*., 2007; Fabre, unpublished thesis). ^{7}Be activity represents the total sum of particulate and dissolved phases (Sommerfield *et al.*, 1999). ^{7}Be activity indicates sediment has been deposited within its detection efficiency, three to five half lives in the past and is a function of suspended sediment, river input and the rates of sediment deposition (Rotondo and Bentley, 2003).

The first analyses preformed on fifty collected grab samples was gamma ray spectrometry, which measures the intensity of gamma radiation versus the energy of each photon (Holmes, 1998). Wet sediment samples were processed immediately upon return to the lab; dried in an oven for a minimum of twelve hours at 60^{o}C, then ground, with visible organics and large pebbles or rocks removed by hand. Wet and dry sample weight measurements were recorded for

porosity calculations. Samples were run individually through a gamma spectrometer using a Canberra Broad Energy Germanium Detector (BEGe) and through Canberry GenieData Software. Collected gamma ray data were processed for a minimum of twenty-four hours each to identify significant spikes of ^{7}Be activity were identified by the signature 477 kilo electron volts (keV) area of the radioisotope. A total of fifty sediment samples were processed for ^{7}Be activity.

^{7}Be measurements found for this study are expressed as disintegrations per minute per grams of sample. The measurements of ^{7}Be activity (dpm/g) were corrected to account for the decay that occurred since the date of sample collection. To find activity when time is zero, cpm/g (counts per minute over grams) divided by cpm/dpm multiplied by the decay to count (minutes between collection and sample analyses).

Grain size analyses were performed on nineteen of the samples, due to the limited quantity of material from remaining collected samples. The possible correlation of grain size selectiveness of radioisotopes was first investigated by He and Walling (1996). This analysis was performed to understand if a correlations exists between grain size and ^{7}Be activity for sediments in karstic basins. Sediment samples analyzed for grain size distribution were prepared and run through the Beckman-Coulter LS 13 320 laser diffractor in the LSU Geology and Geophysics sediment lab. Each sample was run through a one micron sieve to remove large particulates, then rinsed in hydrogen peroxide (H_2O_2) to remove organics. Samples were deflocculated with 10 mL of 0.05% sodium phosphate (NaH_2PO_4) in water to separate individual grains. After each sample was prepared, it was run through the laser diffraction machine for five minutes each to collect the mean and the range of grain sizes. Measured grain sizes are reported here in microns (μ).

To complete the sediment profile, X-Ray Diffraction (XRD) bulk sample analysis was performed on a twenty four of the fifty two grab samples to determine mineral composition.

Samples were run on the Empyrean x-ray diffractometer (PANalytical) (-193^{o}C – 450^{o}C) at the LSU Shared Instrument Facility. This analysis revealed sediment composition before and after peak storm events and differences between sediment composition inside the cave and the surface basin. Samples were homogenized so that the grain sizes of samples would have a better reproducibility on the Reflective Transmission Spinner. The samples were split into two gram fractions and put through a thirty micron sieve, then mixed with 10 mLs of ethanol and run in the micronizer. They were subsequently run through a centrifuge to remove ethanol, then dried overnight at 60^{o}C (Cook *et al.*, 1975).

Samples were analyzed on the XRD by the Reflective Transmission Spinner with the Automatic divergence slit between 4^{o}-70^{o} scans. The scans were done at 0.02 degree increments for 60 seconds. Data were processed through Jade software where detected intensities are identified as peaks. Minerals were normalized against quartz, and mineral intensity factors found (Griffin, 1971). Mineral intensity factors were multiplied by the height of its peak, and all minerals were summed and multiplied by the total to find percentages of mineral composition for each sample.

Table 3. Minerals Actively Sought in this Analysis

Mineral	Window ($^{o}2\theta$)	d spacing (A)	Mineral intensity factor
Quartz	26.45-26.95	3.37-3.31	1
Calcite*	29.25-29.85	3.04-3.01	1.39**
Dolomite*	30.80-31.15	2.90-2.87	1.46**
Total Clay	19.5-20.5	4.55-4.33	20

(Cook *et al.*, 1975)
*Values were reported summed as Carbonates
**Values normalized against quartz by Wanda LeBlanc

CHAPTER IV. RESULTS

4.1 Timing of Hydrologic Events

Daily rainfall data were obtained from January to May, 2014 at three sites and averaged owing to a single site not being located within the boundary of the Gorin Mill sub-basin (Figure 4). The locations of the precipitation monitoring stations are marked on the map in Figure 4 with blue triangles. The first and second weather stations are NOAA monitoring stations at Knob Lick, KY located southeast of Hidden River Cave and at Rex, KY in Hart county located northeast of the catchment area. The third weather station used was the Glasgow airport located south of the study area.

The discharge data were collected from the closest United States Geological Survey (USGS) station 03308500 Green River at the Munfordville, KY, storm monitoring site (Figure 4, site labeled as Munfordville). The monitoring site is approximately ten kilometers north of the Hidden River Cave study site and about five kilometers upstream of the deposition point for the subsurface stream flow into the Green River. Thus, the discharge shown here represents the flow of the Green River during the sample period of April to May of 2014 (Figure 8-9). Discharge of the river shows the highest spikes on 4/5/2014, 4/30/2014, and 5/16/2014. These discharges were 435 m^3/s, 480 m^3/s, and 375 m^3/s, respectively (Figure 9).

Peak rainfall days in the basin were 4/29/2014 and 5/15/2014 during the sampling period. These correspond to peak discharge events occurring on 4/30/2015 and 5/16/2015 at the Green River respectively. The peak discharge event from early April (Figure 8) does not correspond to rainwater from the catchment area of interest possibly meaning that the increased volume of water flow in the Green River at that time corresponds of a storm event upstream of the Horse

Cave area or a malfunction with recording devices, or in an area that does not affect the catchment system.

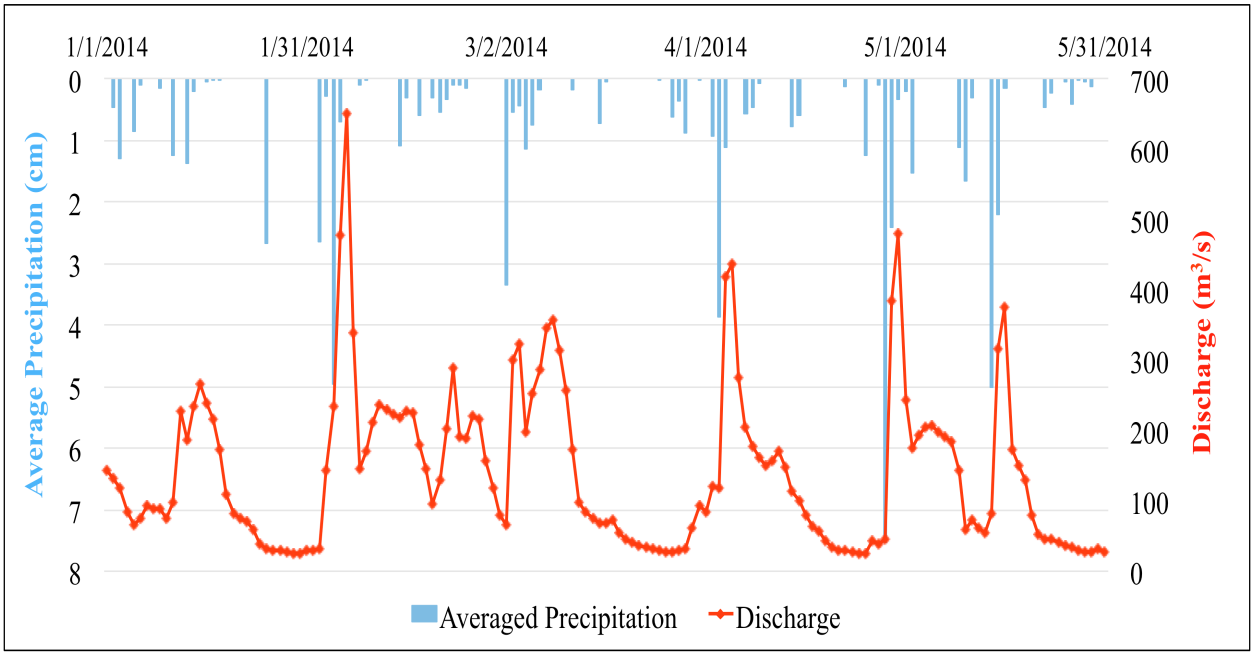

Figure 8. Averaged daily precipitation for the Gorin Mill catchment system for three months before and during the sampling period compared to mean daily discharge from the Green River, KY. Sampling occurred on April 14th-16th, April 31st-May 1st, and May 20th-21st, 2014.

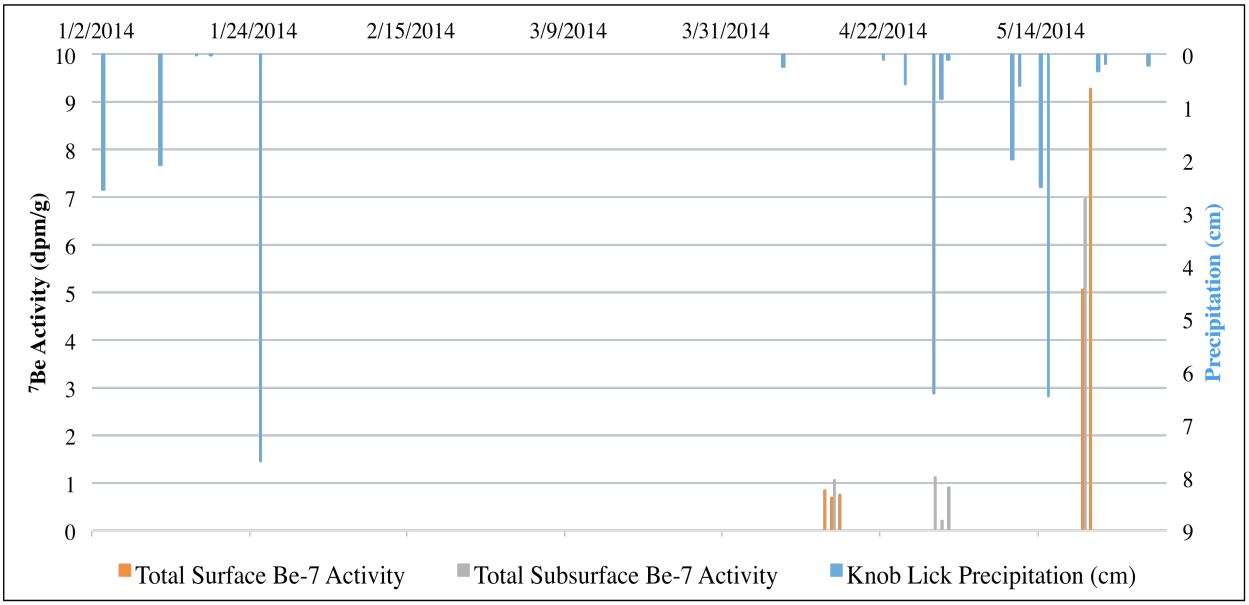

Figure 9. Mean daily precipitation from USGS Knob Lick measuring station compared to the total sampled activity of ^{7}Be from sediment samples at collection date.

4.2 Beryllium-7 Activity of Sediment

The range of measureable ^{7}Be activity of the sediment was 0.04 to 5.37 dpm/g (Table 4). The lowest activities were from sediment samples taken along the Blue Spring Creek tributary on the first sampling trip at the deepest core depths taken from 7.6-15.2 cm and 15.2-25.4 cm. The highest activity measurement was over twice the recorded activity of the next highest sample and this maximum activity was 5.38 dpm/g. This samples was taken from 0 – 1 cm, in the subsurface of Hidden River Cave at water level, upstream of the entrance to the cave at Sb10 in Figure 5 and in Figure 10. The next highest sampled ^{7}Be activity was also from the third sampling trip, it was a 0 – 1 cm sample take on the surface of the basin at S6 on the map in Figure 5. Average ^{7}Be activity for the first (before recharge), second and third (after recharge) sampling trips increased in ascending order and comparison of before and after recharge event activities shown in Figure 10. Average ^{7}Be activity from the first trip was 0.175 dpm/g; second trip average is 0.559 dpm/g; third trip was 0.760 dpm/g. The second sampling trip occurred during a storm event and only subsurface samples were collected. These measured activities correlate to rainfall and discharge data (Figures 8-9). Activity change over time can be described by Equation 2, where A_t is activity at time t (dpm/g), A_o is the initial activity (dpm/g), λ is the decay constant for ^{7}Be, and A_n is new activity (dpm/g):

$$A_t = A_o e^{-\lambda t} + A_n \qquad (2)$$

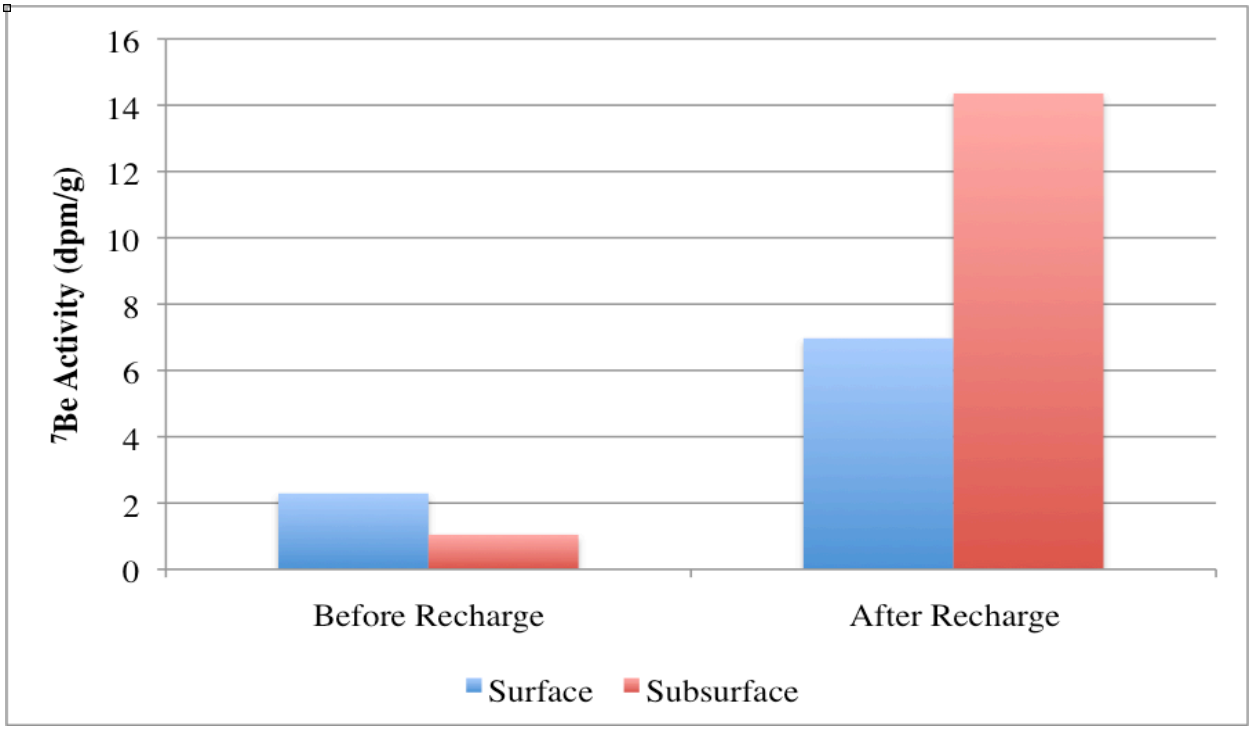

Figure 10. Total ^{7}Be activity measurements from before and after recharge sampling events.

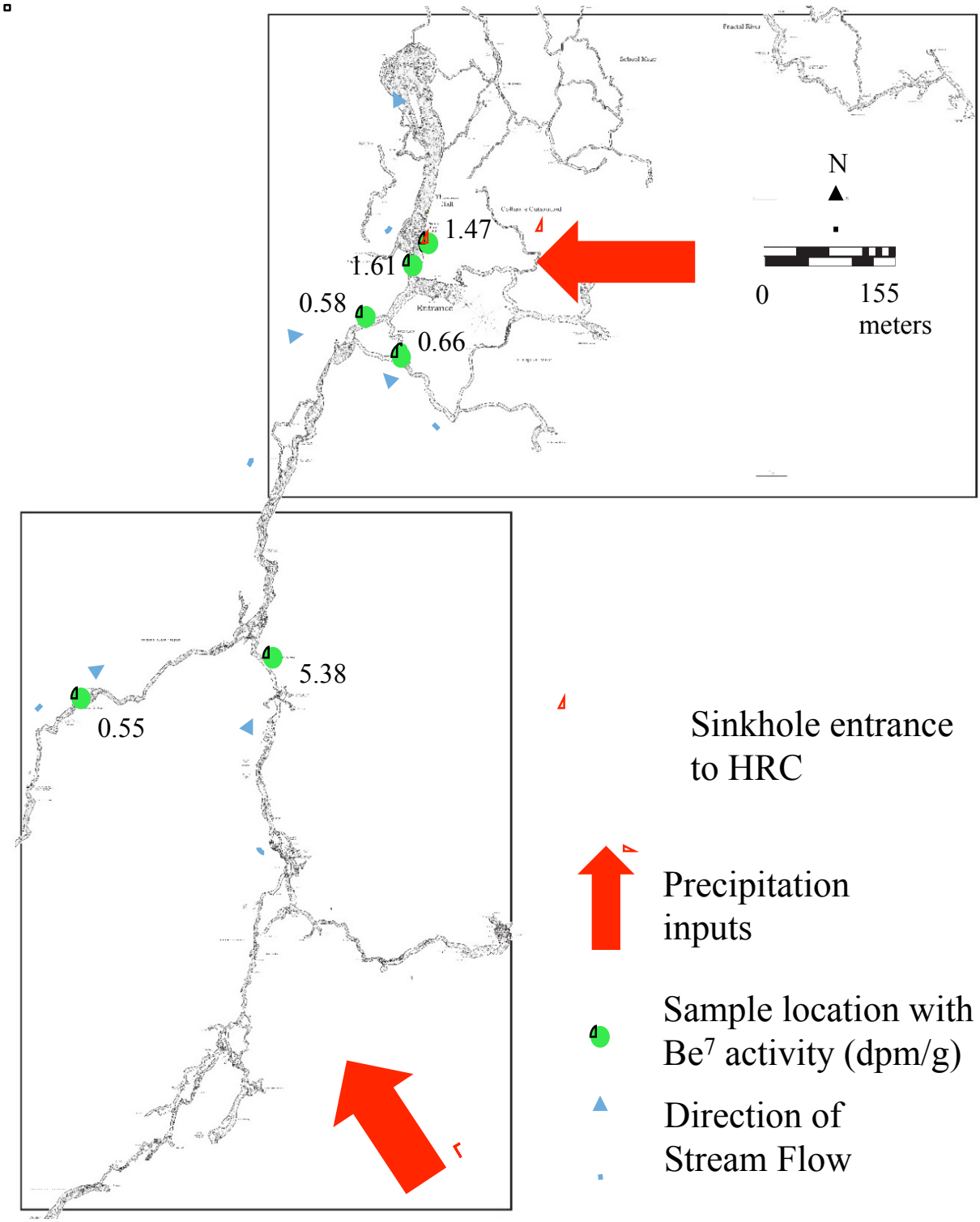

Figure 11. Hidden River Cave map with water level ^{7}Be activities (dpm/g) from after recharge (Modified from West, 2013).

Table 4. ^{7}Be Activity Data and Error

Location	Unique ID (cm)	Collection Date	7Be activity (dpm/g)	Error
S8	0-2.54[1]	4/14/2014	0.34	0.62
S8	2.54-7.62[1]	4/14/2014	0.47	0.43
S8	7.62-15.24[1]	4/14/2014	0.04	8.31
S10	0-2.54[1]	4/15/2014	0.18	0.27
S10	2.54-5.08[1]	4/15/2014	0.38	0.88
S10	5.08-10.16[1]	4/15/2014	0.09	9.69
S10	10.16-15.24[1]	4/15/2014	0.04	19.95
S4	0-2.54[1]	4/16/2014	0.58	0.85
S4	2.54-5.08[1]	4/16/2014	0.17	1.96
Sb3	2.54-5.08[1]	4/15/2014	0.10	1.34
Sb3	10.16-15.24[1]	4/15/2014	0.85	6.77
Sb3	15.24-20.32[1]	4/15/2014	0.10	1.41
Sb6	0-1[1]	4/30/2014	0.22	0.18
Sb9	0-1[1]	5/1/2014	0.91	0.30
Sb2	0-1[2]	4/29/2014	0.62	0.73
Sb5	0-1[1]	4/29/2014	0.50	0.77
Sb7	0-1[2]	5/20/2014	0.52	0.31
Sb3	0-1[1]	5/20/2014	1.47	0.30
Sb4	0-1[2]	5/20/2014	1.61	0.33
Sb8	0-1[3]	5/21/2014	0.66	0.80
Sb11	0-1[3]	5/21/2014	0.55	0.35
Sb9	0-1[2]	5/21/2014	0.17	0.94
Sb9	0-1[3]	5/21/2014	0.58	0.46
Sb10	0-1[2]	5/21/2014	1.95	0.38
Sb10	0-1[3]	5/21/2014	5.38	0.43
Sb1	0-1[4]	5/20/2014	0.41	0.54
Sb1	0-1[4]	5/20/2014	0.62	0.28
Sb1	0-1[4]	5/20/2014	0.15	1.55
Sb1	0-1[4]	5/20/2014	0.33	0.25
S9	0-1[1]	5/20/2014	0.55	0.34
S6	0-1[1]	5/20/2014	2.47	0.34
S2	0-1[1]	5/20/2014	0.24	1.37
S5	0-1[1]	5/20/2014	0.84	0.35
S1	0-1[1]	5/20/2014	1.33	0.36
S4	0-1[1]	5/20/2014	0.93	0.30
S7	0-1[1]	5/20/2014	0.61	0.62

1 Depth of sample in the vertical downhole direction from ground level
2 Taken on at high water mark ledge above water level
3 Taken at water level
4 Taken along a horizontal cross section starting from the base to the top of a large sediment bank. H stands for Height from base 1 to top 6. H2, H3, H4, H5

4.2.1 Uncertainty and Error

A duplicate sample was taken from within the cave at the Sb2 location in the cave from the third sampling event. Both samples were run separately for γ-ray analysis in the laboratory at LSU to measure the variation from potential errors in data due to field and collection processes. However, the field error was unable to be determined because the original and the duplicate sample from Sb2 (Figure 6) were both below detection limits for ^{7}Be.

A sample from the first trip collected near the entrance to Hidden River Cave, at the Sediment Bank from 10-15 cm had an activity level of 0.85 dpm/g on the first run, the second run three weeks later was below detection limits for ^{7}Be. A sample taken within the cave at Sb8 from the third collection trip was run a second twenty four hour count period on the γ-ray analysis to find potential and extent of the error margin. The first run had a measurement of 0.66 dpm/g and the second run was also below the detection limit for ^{7}Be. Therefore laboratory errors were unable to be calculated.

The machine reading error was found for all samples that reported ^{7}Be activity by multiplying the activity (dpm/g) by the error counts and divided by the area of ^{7}Be measured at 477 KeV. The highest errors were found in the deep sections of collected surface samples at the roadside fallow location S8 from 7.6-15 cm and the deepest section of core from S10 at 15-20 cm depth, both samples were collected along the same tributary stream during the first trip. The lowest errors were from samples taken from the surface to 1 cm depth.

4.2.2 Comparisons between sampling events

A total of twenty one unique samples were run for gamma ray spectrometry from the first sampling trip and one sample was run twice, giving twenty two ^{7}Be activity data points from the first trip. The average ^{7}Be activity from the first trip was 0.18 dpm/g.

Ten samples were below detection limits but the remaining twelve data points had measurable data. The range of activity was lowest 0.04 dpm/g at the surface sample collected at Hiseville, Blue Spring Creek 7.6-15 cm section of the core. The highest activity was measured at 0.85 dpm/g in the subsurface at the Sediment Bank 10-15 cm section of the core.

The second trip sediments were collected between 4/29/2014 to 5/1/2014. Only four grab samples were collected at this time and they were exclusively subsurface samples collected from just above flood water levels on the steps and at the entrance. Samples were not collected further into the cave on this trip because floodwaters had filled all previously traversable passages. The average activity measured was 0.56 dpm/g for these samples. The range of activity was lowest at 0.22 dpm/g at Sb6 which was the bottom step into the cave during the receding flood sample from 0 – 1 cm. The high end of the range was 0.91 dpm/g at the sediment drape at the entrance to the south passage of the cave approximately one meter above stream water level at Sb9.

A total of twenty six unique samples were run from the third trip collect between 5/20/2014 to 5/21/2014, with one sample from the Sb8 passage at 0-1 cm run twice. Seven of the twenty seven measured data points were below detection limits for ^{7}Be with the range of activity from 0.12 dpm/g at Sb1, H4, the site of the upstream limit for sampling in the cave. The highest ^{7}Be activity was measured at 5.38 dpm/g and was collected downstream of the entrance of the cave from Sb10 at stream level.

Slight differences exist between from each sampling event between surface and subsurface activity levels (Figure 9). The average of all surface activity is 0.49 dpm/g and average of all subsurface activity is 0.57 dpm/g.

The higher mean radioisotope activity in the subsurface is due to the collection of rainwater in subsurface streams and the subsequent sediment and ^{7}Be carried with it.

The samples taken after peak spring storm events are significantly higher both on the surface and subsurface of the basin.

4.3 Grain Size Analyses Results

A total of nineteen samples were analyzed for grain size, with eight samples from the first trip, two from the second and nine from the third trip (Figure 12). Averages grain sizes are shown in microns (μ) and increased with each trip. The average size from the first trip samples is 46μ, the second trip 48μ and the third trip 83μ.

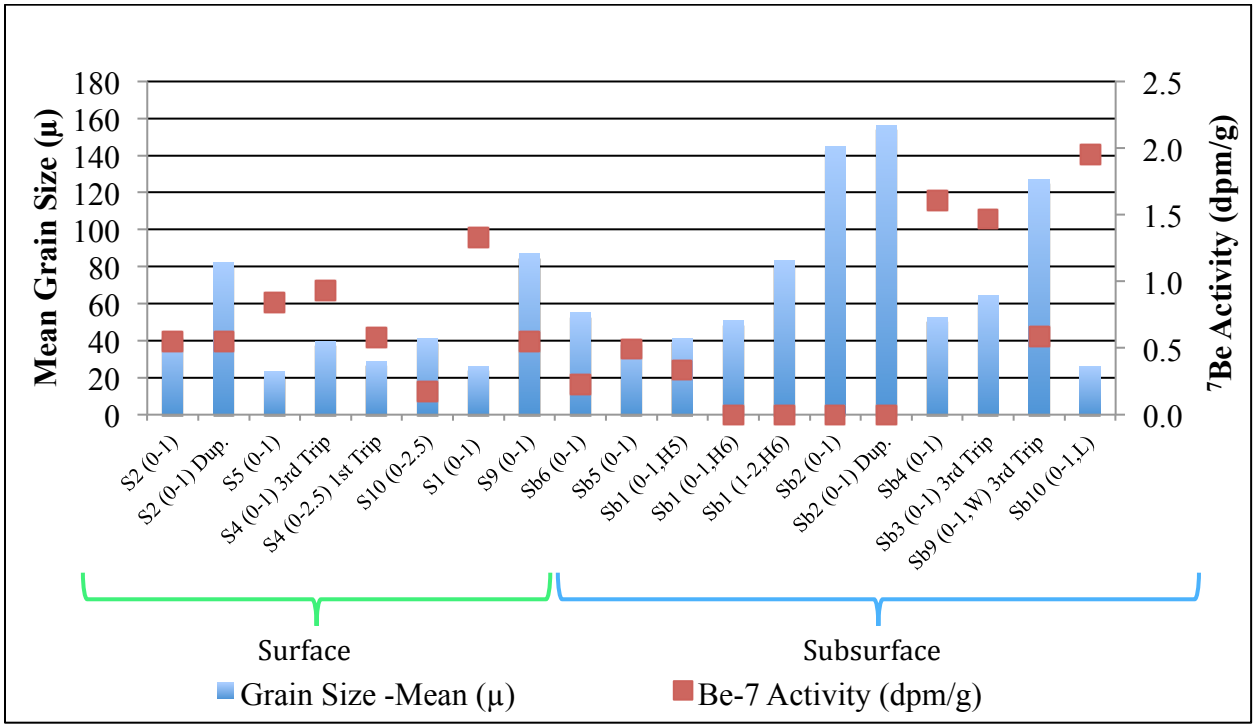

Figure 12. Grain size measurements from a nineteen samples and corresponding ^{7}Be activities.

No correlation was found in the comparison between mean grain size and ^{7}Be activity, so a regression was found to compare how well the data fit with the mean, median and mode of sampled grain size (Figure 12). R^2 values in these regressions range from 0.05 to 0.11 and indicate the mean, median and mode of the grain size do have a strong relationship to the amount of ^{7}Be activity found in samples from this study.

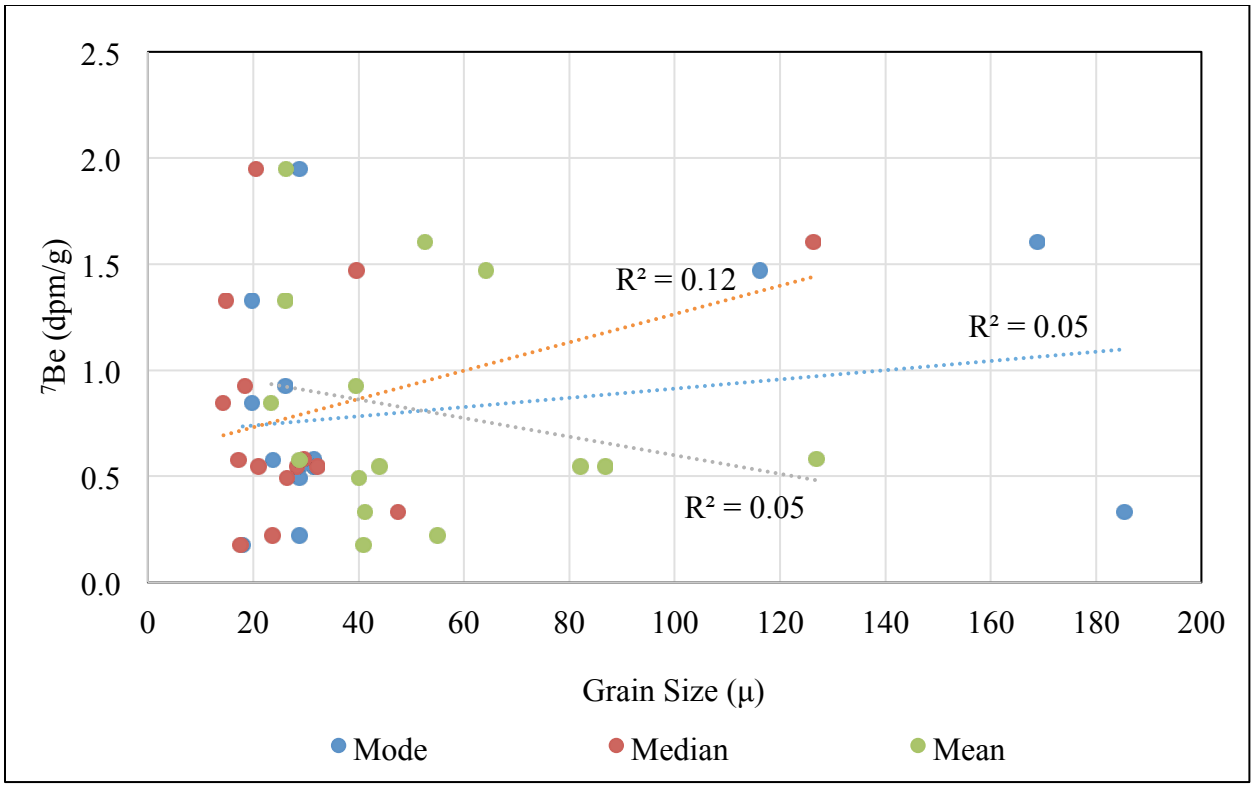

Figure 13. Regression analysis of the Mean, Median and Mode of grain size analysis.

4.4 Whole Sample Mineralogy

Whole sample mineralogical analyses was performed on twenty four samples. Quartz was the dominant sediment component for all samples. In order to understand denudation of carbonate basins by mechanical weathering, I made comparisons between all three sampling events of overall mineralogy and then compared carbonate percentage specifically.

The average percent of carbonates in each sample ranged from the first trip of 0.2% to 3.09% on the third trip. The average amount of carbonate in the samples from the first trip was 0.92%, on the second trip 1.93% and on the third trip 1.9% of the total sediment. Cave samples had higher concentrations of carbonate material (Figure 12). Mineral composition of samples are very similar compared to dissimilar ^{7}Be activity (Figure 13).

The difference in mineral composition shows a slight increase in carbonates from subsurface sediments. The average amount of carbonate per sample on the surface is 0.9% and

1.9% in the subsurface. Average quartz is 88.11% in surface samples and 86.14% in subsurface samples, while total clay was an average of 8.72% on the surface and 10.26% average total clay in subsurface sediments samples.

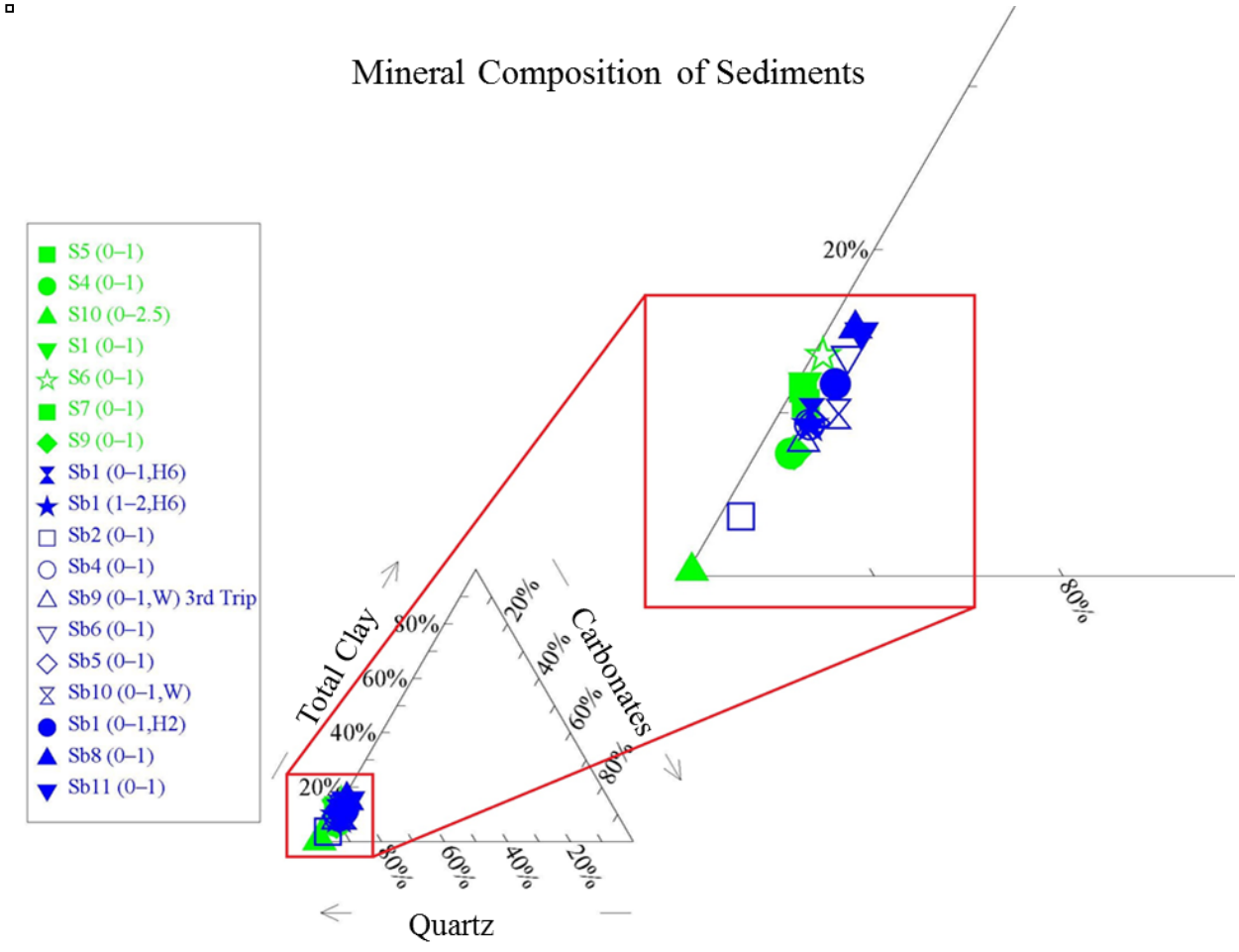

Figure 14. Mineral composition of sediments for a representative number of samples. Green indicates surface samples and blue indicates subsurface samples.

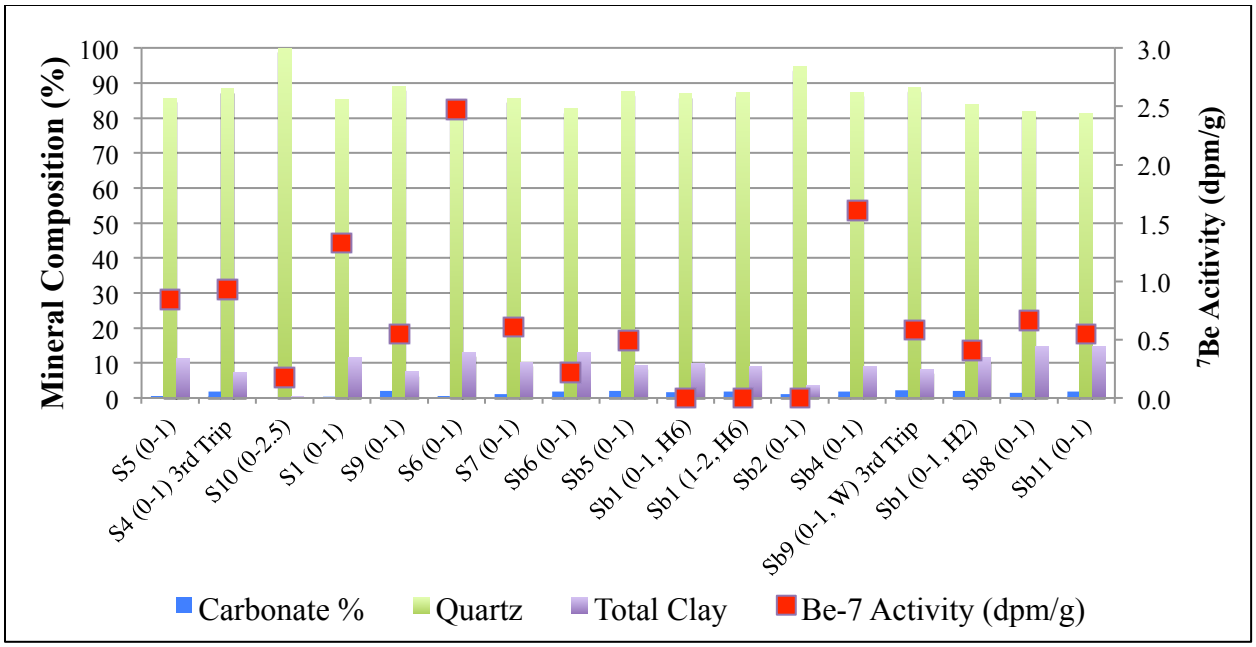

Figure 15. Mineral composition of a representative number of samples compared to corresponding ^{7}Be activity for the selected sample.

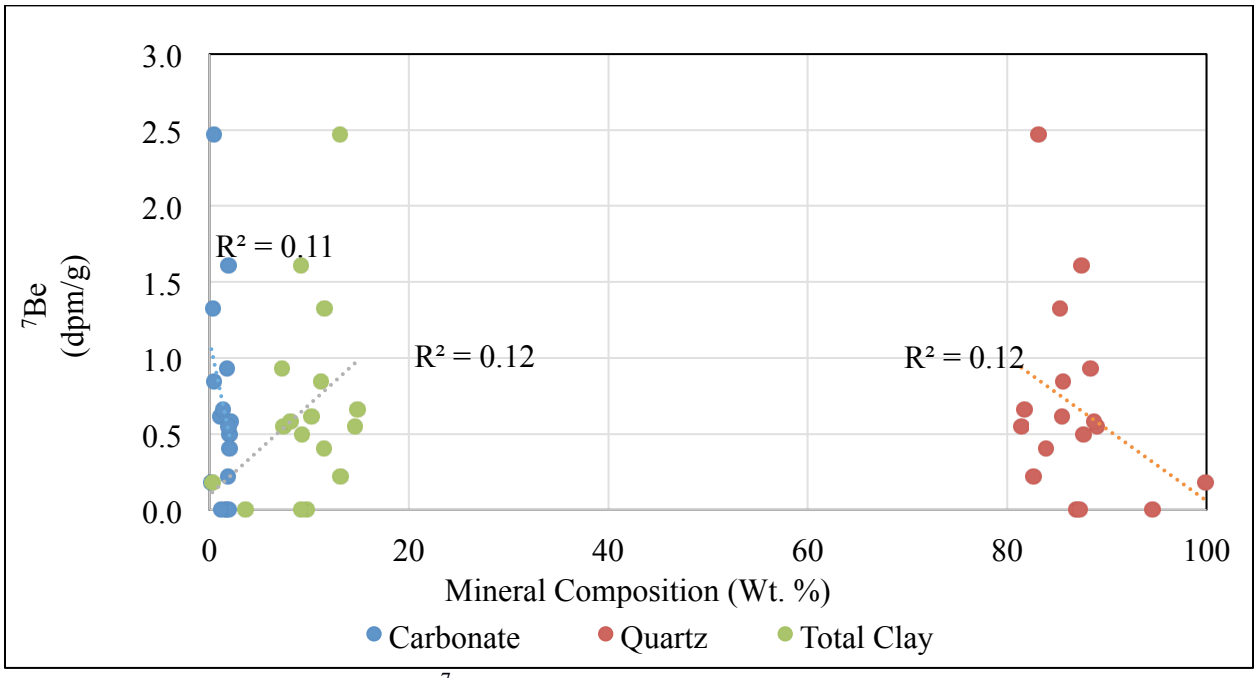

Figure 16. Regression analysis of ^{7}Be activity data and mineral composition of sediments.

CHAPTER V. DISCUSSION

The objective of this work was to determine the validity and application of the radioisotope ^{7}Be to trace sediments over short time scales to understand sediment dynamics in karstic basins. Reference activity levels were found from an initial sampling period before a recharge event. Further sampling occurred during and immediately following several large recharge events. ^{7}Be activities measured from each of these events were compared to understand how effective ^{7}Be can be used to trace sediment dynamics from surface to subsurface systems and if this is a viable method to employ in future studies.

^{7}Be activity measurements for surface systems have been employed extensively in past research and reported values range from 0.9 to 10 dpm/g (Rotondo and Bentley, 2003). A study by Walling (2003) found typical ^{7}Be in overbank sediments from a surface river bank soon after a significant flood to be 6.9 dpm/g and activities from an adjacent field above the level of river inundation to be 2.7 dpm/g. Blake *et al.* (1999) found that for a stable location within the catchment system of interest, typical ^{7}Be to be 3.48 dpm/g, with most activity in the upper few millimeters with exponential decay below that. A study by Sommerfield *et al*. (1999) used anything higher than 3 times the standard deviation for ^{7}Be minimum detection activity (MDA), which for their study was 0.5 dpm/g. A study by Bonniwell *et al*. (1999) used anything less than 53% error for ^{7}Be.

Table 5. Statistical Analysis of ^{7}Be Data

Measurement	Before Recharge In Cave	After Recharge In Cave
Average (dpm/g)	0.35	1.1
Variance (dpm/g)	0.19	1.97
Standard Deviation (dpm/g)	0.43	1.4
P Value	0.06	

The range of detected ^{7}Be activity for cave and surface sediments in this study was 0.04 to 5.37 dpm/g, within the order of magnitude established in previous surface studies and with average activity increasing from before to after recharge. To test the significance of findings the null hypothesis that activity of ^{7}Be after the storm event was equal to ^{7}Be before the storm event, a two sided student t-test was performed. With $\alpha = 0.05$, a 0.06 p value for the null hypothesis was found and the null hypothesis was accepted. With an $\alpha = 0.10$ I was able to reject the null and determined with 94% confidence that before recharge activities were less than after recharge activities (Table 4). To obtain a 95% confidence level, I calculated the necessary sample size needed using Equation 3 below:

$$\text{Necessary Sample Size} = (\text{Z-score})^2 * (1-\sigma)/(\text{margin of error})^2 \qquad (3)$$

where the Z-score for a 95% confidence level is 1.96 and the margin of error is 0.05.
I found that future studies would need ten samples from before recharge within the cave and ten samples after recharge in the subsurface with measured ^{7}Be activities.

Results indicate the upstream cave location at Sb10, is a highly active area for sediment dynamics (Figure 11). This coincides with the larger drainage area of the basin being directed into this passage of the cave (Figure 5). The next most active area of ^{7}Be is immediately downstream of the large sinkhole entrance to the cave in the middle of the town Horse Cave at Sb4 and Sb3. This area is likely active in sediment dynamics and possible rapid geomorphological changes due to the large opening that allows direct rainfall into the cave stream without having to percolate through the overlying sediments or to collect in surface streams and flow into the cave.

The most downstream sampling location at Sb1 consisted of a large sediment pile, activities from the bottom to top were 0.0, 0.41, 0.62, 0.15, 0.33, and 0.0 dpm/g (Table 4). This

closely grouped range of activities in the sediment pile indicated that these activities are essentially the same and result from the most recent recharge event. Areas of the cave stream with low activity measurements are not as active in sediment movement in the short term and have limited expectations for rapid changes.

The hydrologic data illustrate both the correlation between the activities of the ^{7}Be isotope with storm events and validates the effectiveness of the method by showing the lack of storm events preceding our first sampling trip. The effectiveness of ^{7}Be is proven by the absence of significant storm events before our first sampling period that would have brought significant deposition of ^{7}Be through precipitation. Enough time preceded sampling for radioactive decay of ^{7}Be to return to a minimum level of activity at the time of our first sampling trip (Rotondo and Bentley, 2003). The last significant rain or snow storm was roughly three months before our first samples were collected (Figure 9).

Increases in sediment grain size between each successive trip match increased mean ^{7}Be activity for each consecutive sampling event. The mineral compositions of all samples are very similar. Although minimal increased percentages of carbonates in sediment samples from progressive sampling events corresponds to the increased ^{7}Be and subsequently sediment load moving through a karst basin incurred from the recharge event. Large recharge events will weather the limestone layers, causing erosion and movement of the autochthonous carbonate sediment particles.

Future studies could take downhole cores to the penetration depth of ^{7}Be and activity measured within the first half life (~53.3 days), to estimate ^{7}Be inventories and sediment accumulation per day. Sediment accumulation rates (SAR) in the subsurface can be found using equation developed by Muhammed *et al.* (2008). Finding radioisotope inventories can be used to

quantify sediment movement through karst systems (Blake *et al.*, 1999). The amount of sediment deposition from storm events constrains sediment dynamics on short-term time scales. Inventories were not calculated for this research because sampling did not achieve the downhole penetration depth of ^{7}Be activity.

CHAPTER VI. CONCLUSIONS

Due to the short-term hydrologic variation and resulting sediment dynamics observed in karstic basins, the use of a short term natural tracer, ^{7}Be, as a means to determine residence times was investigated. ^{7}Be is a reliable tracer within two to three half-lives (~150 days), so knowing the sediment deposition and residence time within approximately that time is possible (Rotondo and Bentley, 2003). The goal of this study was to determine if ^{7}Be was a viable tracer. The data show that ^{7}Be is useful. If an adequate number of pre-storm samples are collected and if the delay between collection and processing is short, then the confidence in the technique and the data will be higher. These factors would need to be better constrained in future studies but using the ^{7}Be methods pioneered in this investigation will reduce uncertainty in sediment movement and dynamics in karst systems.

REFERENCES

Aley, T., & Fletcher, M. W. (1976). The Water Tracers Cookbook: Missouri Speleology. *Journal of the Missouri Speleological Survey,* 16.

Atkinson, T. C., Smith, D. I., Lavis, J. J., & Whitaker, R. J. (1973). Experiments in tracing underground waters in limestones. *Journal of Hydrology,* 19: 323-349.

Bentley, S. J., Swales, A., Pyenson, B., & Dawe, J. (2014). Sedimentation, bioturbation, and sedimentary fabric evolution on a modern mesotidal mudflat: A multi-tracer study of processes, rates, and scales. *Estuarine, Coastal and Shelf Science,* 141: 58-68.

Blake, W. H., Walling, D. E., & He, Q. (1999). Fallout beryllium-7 as a tracer in soil erosion investigations. *Applied Radiation and Isotopes*, 599-605.

Blake, W. H., Walling, D. E., & He, Q. (2002). Using cosmogenic beryllium-7 as a tracer in sediment budget investigations. *Geografiska Annaler,* 84 A (2): 89-102.

Bonniwell, E. C., Matisoff, G., & Whiting, P. J. (1999). Determining the times and distances of particle transit in a mountain stream using fallout radionuclides. *Geomorphology,* 27: 75-92.

Bosch, R. F., & White, W. B. (2007). Lithofaces and Transport of Clastic Sediments in Karstic Aquifers. In I. D. Sasowksy, & J. Mylroie, *Studies of Cave Sediments* (pp. 1-22). Springer.

Brost, R. A., Feichter, J., & Heimann, M. (1991). Three-Dimensional Simulation of 7Be in a Global Climate Model. *Journal of Geophysical Research, 96*: 22,423-22,445.

Cook, H. E., Johnson, P. D., Matti, J. C., & Zemmels, I. (1975). *Methods of Sample Preperation and X-Ray Diffraction Data Analysis.* Riverside, CA: Initial Reports of the Deep Sea Drilling Project 25.

Corbett, D. R., Dail, M., & McKee, B. (2007). High-frequency time-series of the dynamic sedimentation processes on the western shelf of the Mississippi River Delta. *Continental Shelf Research,* 27: 1600-1615.

Dogwiler, T., & Wicks, C. M. (2004). Sediment entrainment and transport in fluviokarst systems. *Journal of Hydrology*, 295: 163-172.

Drew, D. P., & Smith, D. I. (1969). *Techniques for the tracing of subterranean drainage.* Wokingham, Berkshire United Kingdom: Transport and Road Research Laboratory.

Drew, D. P., & Smith, D. I. (1969). *Techniques for the Tracing of Subterranean Drainage.* Norwich, Norfolk England: Technical Bull No. 2Monograph.

Evrard, O., Nemery, J., Gratiot, N., Duvert, C., Ayrault, S., Lefevre, I., Poulenard, J., Prat, C., Bonte, P., Esteves, M. (2010). Sediment dynamics during the rainy season in tropical

highland catchments of central Mexico using fallout radionuclides. *Geomorphology,* 124: 42-54.

Fabre, J. B. (2012, May). Sediment Flux and Fate for a Large Scale Diversion. *Master's Thesis*. Baton Rouge, Louisiana: LSU Geology and Geophysics.

Gentry, R. W. (Unpublished). ^{7}Be Occurence in Karstic Aquifers with Rapid Flowpaths. *Resesarch Gate.* April 2013. 25 Feb. 2014.

Granger, D. E., & Fabel, D. (2012). Cosmogenic Isotope Dating of Cave Sediments. In W. B. White, & D. C. Culver, *Encylopedia of Caves* (2nd ed., pp. 172-176). Waltham, MA: Academic Press.

Griffin, G. M. (1971). Interpretation of X-Ray Diffraction Data. In R. E. Carver, *Procedures in Sedimentary Petrology* (pp. 541-569). New York: Wiley-Interscience.

Groves, C., & Meiman, J. (2005). Weathering, geomorphic work, and karst landscape evolution in the Cave City groundwater basin, Mammoth Cave, Kentucky . *Geomorphology,* 67: 115-126.

Hans, H. S. (2001). Beta Decay. In H. S. Hans, *Nuclear Physics: Experimental And Theoretical* (pp. 307-369). Daryaganj, New Delhi: New Age International (P) Limited Publishers.

He, Q., & Walling, D. E. (1996). Interpreting Particle Size Effects in the Adsorption of 137Cs and Unsupported 210Pb by Mineral Soils and Sediments. *Journal of Environmental Radioactivity*, 117-137.

Hess, J. W., Wells, S. G., Quilan , J. F., & White, W. B. (1989). Hydrogeology of the South-Central Kentucky Karst. In W. B. White, & E. L. White, *Karst Hydrology Concepts from the Mammoth Cave Area* (pp. 15-64). New York: Van Nostrand Reinhold.

Hess, J. W., & White, W. B. (1989). Chemical Hydrology. In W. B. White, & E. L. White, *Karst Geology Concepts from the Mammoth Cave* (pp. 145-174). New York: Van Nostrand Reinhold.

Holmes, C. W. (1998). *Short-Lived Isotopic Chronometers-A Means of Measuring Decadal Sedimentary Dynamics.* St. Petersburg, FL: U.S. Geological Survey, Department of the Interior.

Junge, C. E. (1963). *Air Chemistry and Radioactivity.* New York: Academic Press.

Livesay, A., & McGrain, P. (1962). *Geology of the Mammoth Cave National Park Area.* Lexington, Kentucky: College of Arts and Sciences, University of Kentucky.

Long, A. J., & Mahler, B. J. (2013). Prediction, time variance, and classification of hydraulic response to recharge in two karst aquifers. *Hydrology and Earth System Sciences*, 17: 281-294.

Loop, C. M., & White, W. B. (2001, January-February). A Conceptual Model for DNAPL Transport in Karst Ground Water Basins. *Ground Water, 39*(1): 119-127.

Lynch, F. L., Mahler, B. J., & Hauwert, N. N. (2004). Provenance of Suspended Sediment Discharged from a Karst Aquifer Determined by Clay Mineralogy. In I. D. Sasowsky, & J. Mylroie, *Studies of Cave Sediments* (pp. 83-93). New York: Springer US.

Mabit, L., Benmansour, M., & Walling, D. E. (2008). Comparative advantages and limitations of the fallout radionuclides 137Cs, 210Pbex. *Journal of Environmental Radioactivity*, 99: 1799–1807.

Mahler, B. J. (1998, September). DNA-labeled clay: A sensitive new method for tracing particle transport. *Geology,* 26(9): 831-834.

Mahler, B. J., Bennett, P. C., & Zimmerman, M. (1998, September-October). Lanthanide-Labeled Clay: A New Method for Tracing Sediment Transport in Karst. *Ground Water,* 36(5): 835-843.

Mahler, B. J., & Long, A. J. (2013). Prediction, time variance, and classification of hydraulic response to recharge in two karst aquifers. *Hydrology and Earth System Sciences,* 17: 281-294.

Mahler, B. J., & Lynch, F. L. (1999). Muddy waters: temporal variation in sediment discharging from a karst spring. *Journal of Hydrology*, 214: 165-178.

May, M. T., Kuehn, K. W., & Siewers, F. D. (2007). (unpublised guide) Geology of the Mammoth Cave and Nolin River Gorge Region with Emphasis on Hydrocarbon and Karst Resources.

Muhammad, Z., Bentley, S. J., Febo, L. A., Droxler, A. W., Dickens, G. R., Peterson, L. C. and Opdyke, B. N. (2008), Excess ^{210}Pb inventories and fluxes along the continental slope and basins of the Gulf of Papua, *J. Geophys. Res.* 113: F01S17, doi: 10.1029/2006JF0000676.

Murray, A. S., Stanton, R., Olley, J. M., & Morton, R. (1993). Determining the origins and history of sedimentation in an underground river system using natural and fallout radionuclides. *Journal of Hydrology,* 146: 341-359.

Palmer, A. M. (1991, January). Origin and morphology of limestone caves. *Geological Society of America Bulletin,* 103: 1-21.

Palmer, A. N. (2012). Passage and Growth Development. In W. B. White, & D. C. Culver, *Encyclopedia of Caves* (pp. 598-603). Elsevier.

Rotondo, K. A., & Bentley, S. J. (2003). Deposition and Resuspension of Fluid Mud on the Western Louisiana Inner Shelf. *GCAGS/GCSSEPM Transactions,* 53: 722-731.

Russell, W. L. (1932). Geology of Oil and Gas Fields of Western Kentucky. *American Association of Petroleum Geologists,* 16(3): 231-254.

Sommerfield, C. K., Nittrouer, C. A., & Alexander, C. R. (1999). 7Be as a tracer of flood sedimentation on the northern California continental margin. *Continental Shelf Research,* 19: 335-361.

Stock, G. M., Granger, D. E., Sasowsky, I. D., Anderson, R. S., & Finkel, R. C. (2005). Comparison of U–Th, paleomagnetism, and cosmogenic burial methods for dating caves: Implications for landscape evolution studies. *Earth and Planetary Science Letters,* 236: 388-403.

Thornberry-Ehrlich, T. (2011). *Mammoth Cave National Park: Geologic Resources Inventory Report.* Fort Collins, Colorado: National Park Service.

Toomey, R. S., & Olson, R. (2008). *Field Trip Guide Mammoth Cave National Park Tour.* Mammoth Cave, KY.

Walling, D. E. (2003). Using Environmental Radionuclides in Sediment Budget Investigations. (pp. 57-78). Oslo: IAHS Publication.

Walling, D. E. (2013). Beryllium-y: The Cinderella of fallout radionuclide sediment tracers? *Hydrological Processes*, 27: 830-844.

Walsh, K. A. (2009). Introduction. In K. A. Wlash, *Beryllium Chemistry and Processing* (pp. 1-5). Materials Park, OH: ASM International.

West, D. (2013). Hidden River Cave. *Sunset Dome and Rimstone Maze.* Cave Research Foundation, Horse Cave, Kentucky. 1 Map.

White, W. B. (1989). Introduction to the Karst Hydrology of the Mammoth Cave Area. In W. B. White, & E. L. White, *Karst Hydrology* (pp. 1-14). New York: Van Nostrand Reinhold.

APPENDIX A: GAMMA RAY SPECTROMETRY DATA

Sample ID:	Depth (cm)	Wet wt.	Dry wt.	% Water
S8 (0-2.5)	0-2.54	57.70	42.06	27.11
S8 (2.5-7.5)	2.54-7.62	73.23	54.18	26.01
S8 (7.5-15)	7.62-15.24	83.16	65.41	21.34
S8 (15-25)	15.24-25.4	100.24	81.00	19.19
S10 (0-2.5)	0-2.54	68.55	47.97	30.02
S10 (2.5-5)	2.54-5.08	66.32	49.47	25.41
S10 (5-10)	5.08-10.16	90.27	70.60	21.79
S10 (10-15)	10.16-15.24	66.89	53.63	19.82
S10 (15-20)	15.24-20.32	92.80	75.03	19.15
S4 (0-2.5) 1st Trip	0-2.54	58.70	43.43	26.01
S4 (2.5-5) 1st Trip	2.54-5.08	61.50	47.22	23.22
S4 (5-10) 1st Trip	5.08-10.16	69.90	54.80	21.60
S4 (10-15) 1st Trip	10.16-15.24	66.64	53.51	19.70
S4 (15-20) 1st Trip	15.24-20.32	70.66	57.22	19.02
S4 (20-25) 1st Trip				
Sb3 (0-2.5) 1st Trip	0-2.54	126.60	92.99	26.55
Sb3 (2.5-5) 1st Trip	2.54-5.08	182.80	133.40	27.02
Sb3 (5-10) 1st Trip	5.08-10.16	154.60	115.30	25.42
Sb3 (10-15) 1st Trip	10.16-15.24	139.80	104.71	25.10
Sb3 (10-15) 2nd Run	10.16-15.24	139.80	104.71	25.10
Sb3 (15-20) 1st Trip	15.24-20.32	154.30	116.50	24.50
Sb3 (20-25) 1st Trip	20.32-25.4	167.50	122.80	26.69
Sb6 (0-1)	0-1	79.64	49.23	38.18
Sb9 (0-1) 2nd Trip	0-1	96.97	61.79	36.28
Sb2 (0-1) 2nd Trip	0-1	79.85	54.96	31.17
Sb5 (0-1)	0-1	66.57	34.86	47.63
Sb5 (0-1) 2nd Run	0-1	66.57	34.86	
Sb5 (0-1) Run incorrectly	0-1	66.57	34.86	
Sb7 (0-1)	0-1	66.50	43.04	35.28
Sb3 (0-1) 3rd Trip	0-1	92.97	63.78	31.40
Sb4 (0-1)	0-1	61.80	39.30	36.41
Sb2 (0-1) 3rd Trip	0-1	71.54	60.06	16.05
Sb2 (0-1) 2nd Run	0-.5	50.00	40.49	19.02
Sb8 (0-1)	0-1	81.88	55.82	31.83
Sb8 (0-1) 2nd Run	0-1	81.88	55.82	31.83
Sb11 (0-1)	0-1	84.69	61.57	27.30
Sb9 (0-1, L) 3rd Trip	0-1	78.00	58.14	25.46

Sample ID:	Depth (cm)	Wet wt.	Dry wt.	% Water
Sb9 (0-1, W) 3rd Trip	0-1	97.74	74.47	23.81
Sb10 (0-1, L)	0-1	67.13	47.85	28.72
Sb10 (0-1, W)	0-1	61.62	40.24	34.70
Sb1 (0-1, H1)	0-1	120.36	85.77	28.74
Sb1 (0-1, H2)	0-1	86.72	62.65	27.76
Sb1 (0-1, H3)	0-1	87.13	63.76	26.82
Sb1 (0-1, H4)	0-1	121.96	87.10	28.58
Sb1 (0-1, H5)	0-1	74.63	52.16	30.11
Sb1 (0-1, H6_	0-1	95.35	67.72	28.98
Sb1 (1-2, H6)	1-2	74.72	53.50	28.40
Sb1 (2-3, H6)	2-3	140.10	100.20	28.48
S2 (0-1)	0-1	47.92	39.12	18.36
S6 (0-1)	0-1	56.46	52.31	7.35
S9 (0-1)	0-1	34.05	25.54	24.99
S5 (0-1)	0-1	51.09	42.62	16.58
S1 (0-1)	0-1	44.92	40.21	10.49
S4 (0-1) 3rd Trip	0-1	50.66	39.35	22.33
S7 (0-1)	0-1	59.14	51.04	13.70

Sample ID:	Porosity	DBD	Count Mass	Collection Date	Count Date	Count Time (s)	Count (minutes)
S8 (0-2.5)	0.49	1.32	15.65	4/14/2014	4/30/2014	86390.7	23040
S8 (2.5-7.5)	0.48	1.36	17.46	4/14/2014	5/1/2014	86390.9	24480
S8 (7.5-15)	0.41	1.52	13.93	4/14/2014	5/2/2014	86391.3	25920
S8 (15-25)	0.38	1.61	16.92	4/14/2014	5/5/2014	86390.9	30240
S10 (0-2.5)	0.53	1.23	14.91	4/15/2014	5/10/2014	86390.9	36000
S10 (2.5-5)	0.47	1.38	15.99	4/15/2014	5/16/2014	86390.9	44640
S10 (5-10)	0.42	1.51	20.15	4/15/2014	5/17/2014	80213.3	46080
S10 (10-15)	0.39	1.58	18.46	4/15/2014	7/1/2014	84997.3	110880
S10 (15-20)	0.38	1.61	20.17	4/15/2014	7/2/2014	85096.6	112320
S4 (0-2.5) 1st Trip	0.48	1.36	12.97	4/16/2014	5/15/2014	86391.1	41760
S4 (2.5-5) 1st Trip	0.44	1.46	15.59	4/16/2014	5/12/2014	86390.6	37440
S4 (5-10) 1st Trip	0.42	1.51	15.45	4/16/2014	5/18/2014	86390.6	46080
S4 (10-15) 1st Trip	0.39	1.59	17.62	4/16/2014	6/30/2014	87839.4	108000
S4 (15-20) 1st Trip	0.38	1.61	17.34	4/16/2014	7/1/2014	85001.2	109440
S4 (20-25) 1st Trip			17.98				
Sb3 (0-2.5) 1st Trip	0.48	1.34	19.20	4/15/2014	4/17/2014	86391.5	2880
Sb3 (2.5-5) 1st Trip	0.49	1.32	17.73	4/15/2014	4/18/2014	86391	4320
Sb3 (5-10) 1st Trip	0.47	1.38	21.26	4/15/2014	4/19/2014	84591.5	5760
Sb3 (10-15) 1st Trip	0.47	1.39	15.17	4/15/2014	4/20/2014	8908.3	7200
Sb3 (10-15) 2nd Run	0.47	1.39	15.17	4/15/2014	5/6/2014	86391.3	30240
Sb3 (15-20) 1st Trip	0.46	1.41	18.96	4/15/2014	4/20/2014	86390.9	7200
Sb3 (20-25) 1st Trip	0.49	1.34	17.62	4/15/2014	4/21/2014	83691.6	8640
Sb6 (0-1)	0.62	1.00	18.35	4/30/2014	5/25/2014	86390.8	
Sb9 (0-1) 2nd Trip	0.60	1.05	17.16	5/1/2014	5/24/2014	86390.8	33120
Sb2 (0-1) 2nd Trip	0.54	1.19	14.67	4/29/2014	5/26/2014	80092.1	38880

Sample ID:	Porosity	DBD	Count Mass	Collection Date	Count Date	Count Time (s)	Count (minutes)
Sb5 (0-1)	0.70	0.77	15.68	4/29/2014	5/28/2014	86390.1	41760
Sb5 (0-1) 2nd Run			15.68	4/29/2014	5/30/2014	86400	
Sb5 (0-1) Run incorrectly			15.68	4/29/2014	6/17/2014		70560
Sb7 (0-1)	0.59	1.08	17.30	5/20/2014	6/17/2014	86390.7	40320
Sb3 (0-1) 3rd Trip	0.54	1.19	15.72	5/20/2014	6/19/2014	89504.6	43200
Sb4 (0-1)	0.60	1.04	15.22	5/20/2014	6/20/2014	98004.7	44640
Sb2 (0-1) 3rd Trip	0.33	1.74	18.12	5/20/2014	6/17/2014	86400	40320
Sb2 (0-1) 2nd Run	0.38	1.61	18.26	5/20/2014	6/25/2014	138000	51840
Sb8 (0-1)	0.55	1.17	14.09	5/21/2014	6/25/2014	86390.4	50400
Sb8 (0-1) 2nd Run	0.55	1.17	14.09	5/21/2014	6/26/2014	86390.4	51840
Sb11 (0-1)	0.49	1.32	16.97	5/21/2014	6/30/2014	86390.1	57600
Sb9 (0-1, L) 3rd Trip	0.47	1.38	17.65	5/21/2014	6/22/2014	138000	46080
Sb9 (0-1, W) 3rd Trip	0.45	1.43	19.06	5/21/2014	6/21/2014	88802	44640
Sb10 (0-1, L)	0.51	1.27	15.15	5/21/2014	6/19/2014	84991.8	41760
Sb10 (0-1, W)	0.58	1.09	15.52	5/21/2014	6/18/2014	80492.5	40320
Sb1 (0-1, H1)	0.51	1.27	16.74	5/20/2014	6/2/2014	85205.8	18720
Sb1 (0-1, H2)	0.50	1.30	15.64	5/20/2014	6/1/2014	86400	17280
Sb1 (0-1, H3)	0.49	1.33	17.63	5/20/2014	6/3/2014	86400	20160
Sb1 (0-1, H4)	0.51	1.27	18.13	5/20/2014	6/4/2014	85402.6	21600
Sb1 (0-1, H5)	0.53	1.23	16.18	5/20/2014	6/5/2014	86400	23040
Sb1 (0-1, H6_	0.51	1.26	17.51	5/20/2014	6/12/2014	86400	33120
Sb1 (1-2, H6)	0.51	1.28	14.10	5/20/2014	6/13/2014	86400	34560
Sb1 (2-3, H6)	0.51	1.28	16.34	5/20/2014	6/16/2014	86400	38880

Sample ID:	Porosity	DBD	Count Mass	Collection Date	Count Date	Count Time (s)	Count (minutes)
S2 (0-1)	0.37	1.64	19.14	5/20/2014	6/6/2014	86390.3	24480
S6 (0-1)	0.17	2.16	16.74	5/20/2014	6/5/2014	86390.3	23040
S9 (0-1)	0.46	1.39	14.28	5/20/2014	6/4/2014	86390.2	21600
S5 (0-1)	0.34	1.71	16.39	5/20/2014	6/13/2014	86390.5	34560
S1 (0-1)	0.23	1.99	13.67	5/20/2014	6/12/2014	86390.6	33120
S4 (0-1) 3rd Trip	0.43	1.49	16.68	5/20/2014	6/3/2014	86390.4	20160
S7 (0-1)	0.29	1.84	15.54	5/20/2014	6/16/2014	86390.4	38880

Sample ID	^{7}Be 477 kev Area	error cts	^{7}Be Lambda,Be-7 1/min	cpm/dpm	cpm/g	Decay to count
S8 (0-2.5)	28	50.33	9.031E-06	0.00446	0.00124259	0.81
S8 (2.5-7.5)	42	39.04	9.031E-06	0.00446	0.001670661	0.80
S8 (7.5-15)	3	588.44	9.031E-06	0.00446	0.000149572	0.79
S8 (15-25)	0	0.00		0.00446	0	1
S10 (0-2.5)	12	18.95	9.031E-06	0.00446	0.000568284	0.72
S10 (2.5-5)	26	60.54	9.031E-06	0.00446	0.001129297	0.67
S10 (5-10)	0	0.00	9.031E-06	0.00446	0	0.66
S10 (10-15)	4	415.10	9.031E-06	0.00446	0.000152959	0.37
S10 (15-20)	2	922.92	9.031E-06	0.00446	6.99138E-05	0.36
S4 (0-2.5) 1st Trip	33	48.33	9.031E-06	0.00446	0.00176708	0.69
S4 (2.5-5) 1st Trip	12	139.68	9.031E-06	0.00446	0.000534589	0.71
S4 (5-10) 1st Trip	0	0.00	9.031E-06	0.00446	0	0.66
S4 (10-15) 1st Trip	0	0.00	9.031E-06	0.00446		0.38
S4 (15-20) 1st Trip	N/A	N/A	9.031E-06	0.00446		0.37
S4 (20-25) 1st Trip						
Sb3 (0-2.5) 1st Trip	0	0.00	9.031E-06	0.00446	0	0.97
Sb3 (2.5-5) 1st Trip	11	147.23	9.031E-06	0.00446	0.00043089	0.96
Sb3 (5-10) 1st Trip	0	0.00	9.031E-06	0.00446	0	0.95
Sb3 (10-15) 1st Trip	8	63.74	9.031E-06	0.00446	0.003551901	0.94
Sb3 (10-15) 2nd Run	0	0.00	9.031E-06	0.00446	0	0.76
Sb3 (15-20) 1st Trip	11	161.09	9.031E-06	0.00446	0.000402937	0.94
Sb3 (20-25) 1st Trip	0	0.00	9.031E-06	0.00446	0	0.92
Sb6 (0-1)	26	20.59	9.031E-06	0.00446	0.000987844	1
Sb9 (0-1) 2nd Trip	74	24.17	9.031E-06	0.00446	0.002995009	0.74
Sb2 (0-1) 2nd Trip	38	45.06	9.031E-06	0.00446	0.001940506	0.70

Sample ID	^{7}Be 477 kev Area	error cts	^{7}Be Lambda, Be-7 1/min	cpm/dpm	cpm/g	Decay to count
Sb5 (0-1)	34	53.02	9.031E-06	0.00446	0.001505983	0.69
Sb5 (0-1) 2nd Run	77	23.58				
Sb5 (0-1) Run incorrectly	17	110.52				
Sb7 (0-1)	40	23.77	9.031E-06	0.00446	0.001605825	0.69
Sb3 (0-1) 3rd Trip	104	21.07	9.031E-06	0.00446	0.004434929	0.68
Sb4 (0-1)	119	24.50	9.031E-06	0.00446	0.004786705	0.67
Sb2 (0-1) 3rd Trip	0	0.00	9.031E-06	0.00446	0	0.69
Sb2 (0-1) 2nd Run	0	0.00	9.031E-06	0.00446	0	0.63
Sb8 (0-1)	38	45.62	9.031E-06	0.00446	0.001873089	0.63
Sb8 (0-1) 2nd Run	0	0.00	9.031E-06	0.00446	0	0.63
Sb11 (0-1)	35	22.42	9.031E-06	0.00446	0.001448801	0.59
Sb9 (0-1, L) 3rd Trip	20	111.77	9.031E-06	0.00446	0.000492672	0.66
Sb9 (0-1, W) 3rd Trip	49	38.3	9.031E-06	0.00446	0.001737007	0.67
Sb10 (0-1, L)	128	24.8	9.031E-06	0.00446	0.005964466	0.69
Sb10 (0-1, W)	347	27.75	9.031E-06	0.00446	0.016666085	0.69
Sb1 (0-1, H1)	0	0.00	9.031E-06	0.00446	0	0.84
Sb1 (0-1, H2)	35	46.07	9.031E-06	0.00446	0.001554064	0.86
Sb1 (0-1, H3)	59	26.02	9.031E-06	0.00446	0.002304311	0.83
Sb1 (0-1, H4)	11	146.59	9.031E-06	0.00446	0.00042626	0.82
Sb1 (0-1, H5)	28	21.00	9.031E-06	0.00446	0.001201758	0.81
Sb1 (0-1, H6_	0	0.00	9.031E-06	0.00446	0	0.74
Sb1 (1-2, H6)	0	0.00	9.031E-06	0.00446	0	0.73
Sb1 (2-3, H6)	0	0.00	9.031E-06	0.00446	0	0.70
S2 (0-1)	54	33.79	9.031E-06	0.00446	0.001959468	0.80
S6 (0-1)	216	29.45	9.031E-06	0.00446	0.00896158	0.81
S9 (0-1)	18	103.70	9.031E-06	0.00446	0.000875449	0.82
S5 (0-1)	65	26.60	9.031E-06	0.00446	0.002754353	0.73
S1 (0-1)	87	23.56	9.031E-06	0.00446	0.004394732	0.74
S4 (0-1) 3rd Trip	83	26.59	9.031E-06	0.00446	0.003447625	0.83
S7 (0-1)	43	43.52	9.031E-06	0.00446	0.001921778	0.70

APPENDIX B: GRAIN SIZE DATA

Sample Number	Mean (μ)	Mode (μ)	Median (μ)	Standard Deviation (μ)
S9 (0-1)	43.89	31.50	20.94	54.46
S9 (0-1) Dup.	82.05	31.50	28.31	140.09
S5 (0-1)	23.44	19.76	14.34	29.80
S4 (0-1) 3rd Trip	39.46	26.14	18.39	56.64
S4 (0-2.5) 1st Trip	28.74	23.81	17.25	39.20
S10 (0-2.5)	40.96	18.00	17.63	53.79
S1(0-1)	26.05	19.76	14.83	34.10
S2 (0-1)	86.89	28.69	32.21	115.40
Sb1 (0-1, H5)	41.11	28.69	23.69	47.17
Sb1 (0-1, H6)	50.59	28.69	26.47	57.11
Sb1 (1-2, H6)	83.13	185.37	47.49	75.17
Sb2 (0-1) 3rd Trip	144.83	203.49	152.09	95.23
Sb2 (0-1) 3rd Trip, Dup.	156.29	223.38	165.52	112.42
Sb4 (0-1)	52.60	31.50	33.02	51.97
Sb3 (0-1) 3rd Trip	64.26	127.64	46.20	57.64
Sb9 (0-1) 2nd Trip	126.90	168.86	126.36	92.13
Sb6 (0-1)	54.99	116.28	39.53	45.90
Sb5 (0-1)	40.09	31.50	29.62	34.94
Sb10 (0-1, L)	26.27	28.69	20.47	23.26

APPENDIX C: XRD DATA

Caroline's Sample Number	Carbonate	Quartz	Total Clay	Sum
S5 (0-1)	0.48	85.62	11.18	97.28
S4 (0-1) 3rd Trip	1.78	88.35	7.3	
S4 (0-2.5) 1st Trip				
S10 (0-2.5)	0.2	99.88	0.3	100.38
S1(0-1)	0.38	85.26	11.55	97.19
S2 (0-1)	1.98	88.99	7.44	98.41
Sb1 (0-1, H5)				0
Sb1 (0-1, H6)	1.67	86.9	9.81	98.38
Sb1 (1-2, H6)	1.92	87.28	9.13	98.33
Sb2 (0-1) 3rd Trip	1.11	94.61	3.63	99.35
Sb2 (0-1) 3rd Trip, Dup.				0
Sb4 (0-1)	1.92	87.43	9.14	98.5
Sb3 (0-1) 3rd Trip				0
Sb9 (0-1) 2nd Trip	2.13	88.74	8.14	99.02
Sb6 (0-1)	1.81	82.67	13.14	97.62
Sb5 (0-1)	2.03	87.65	9.29	98.98
Sb10 (0-1, L)	3.09	85.1	9.72	97.91
S6 (0-1)	0.51	83.15	13.07	96.73
S7 (0-1)	1.06	85.55	10.24	96.86
Sb1 (0-1, H2)	2.00	83.96	11.47	97.44
Sb8 (0-1)	1.39	81.77	14.85	98.01
Sb11 (0-1)	1.82	81.44	14.64	97.90

APPENDIX D: HYDROLOGY AND TOTAL ^{7}BE ACTIVITIES DATA

Date	Total Surface ^{7}Be Activity	Total Subsurface ^{7}Be Activity	Discharge (m^3/s)
4/1/2014			84.38
4/2/2014			121.48
4/3/2014			118.93
4/4/2014			419.09
4/5/2014			436.08
4/6/2014			275.24
4/7/2014			203.88
4/8/2014			178.11
4/9/2014			161.69
4/10/2014			149.8
4/11/2014			156.31
4/12/2014			170.47
4/13/2014			146.96
4/14/2014	0.85		113.55
4/15/2014	0.69	1.05	99.96
4/16/2014	0.75		80.42
4/17/2014			63.15
4/18/2014			56.07
4/19/2014			43.32
4/20/2014			33.98
4/21/2014			30.3
4/22/2014			28.60
4/23/2014			27.27
4/24/2014			25.55
4/25/2014			25.60
4/26/2014			43.61
4/27/2014			37.66
4/28/2014			45.59
4/29/2014		1.11	385.11
4/30/2014		0.22	481.39
5/1/2014		0.91	242.96
5/2/2014			175.56
5/3/2014			192.55
5/4/2014			205.58
5/5/2014			208.13
5/6/2014			198.78

Date	Total Surface ^{7}Be Activity	Total Subsurface ^{7}Be Activity	Discharge (m^3/s)
5/7/2014			191.42
5/8/2014			185.19
5/9/2014			142.43
5/10/2014			58.62
5/11/2014			73.34
5/12/2014			62.01
5/13/2014			54.65
5/14/2014			81.55
5/15/2014			317.15
5/16/2014			376.61
5/17/2014			173.02
5/18/2014			150.93
5/19/2014			130.82
5/20/2014	5.07	6.97	80.14
5/21/2014	9.29		53.24
5/22/2014			46.44
5/23/2014			45.59
5/24/2014			39.93
5/25/2014			35.68
5/26/2014			33.41
5/27/2014			29.45
5/28/2014			28.32
5/29/2014			28.20
5/30/2014			32.00
5/31/2014			28.26

Knob Lick Precipitation (in)	Rex Precipitation (in)	Glasgow Airport Precipitation	Date	Average Precipitation (cm)	Discharge (m^3/s)
	0		1/1/2014		143.57
	0.18	0.18	1/2/2014	0.46	131.67
1.01	0		1/3/2014	1.28	117.80
	0		1/4/2014	0	84.95
	N/A	0.33	1/5/2014	0.84	65.13
	N/A	0.04	1/6/2014	0.10	75.61
	N/A		1/7/2014		93.73
	N/A		1/8/2014		89.76
	N/A	0.06	1/9/2014	0.15	88.07
	N/A		1/10/2014		75.61
0.83	0	0.63	1/11/2014	1.24	96.84
			1/12/2014		227.10
	0.48	0.59	1/13/2014	1.36	186.32
	0.14	0.02	1/14/2014	0.20	233.61
			1/15/2014		266.74
0.01	0.02	0.02	1/16/2014	0.04	239.84
	0.01		1/17/2014	0.03	215.21
0.01			1/18/2014	0.03	173.87
			1/19/2014		109.59
			1/20/2014		82.40
			1/21/2014		75.61
			1/22/2014		69.66
			1/23/2014		59.75
			1/24/2014		37.94
3.03	0.1	0.02	1/25/2014	2.67	32.28
			1/26/2014		30.58
			1/27/2014		28.60
			1/28/2014		26.99
			1/29/2014		26.14
			1/30/2014		25.66
			1/31/2014		28.60
			2/1/2014		29.73
	0.85	1.22	2/2/2014	2.6289	31.15
	0.19	0.02	2/3/2014	0.2667	143.85
		1.95	2/4/2014	4.953	235.31
	0.49	0.05	2/5/2014	0.6858	478.55

Knob Lick Precipitation (in)	Rex Precipitation (in)	Glasgow Airport Precipitation	Date	Average Precipitation (cm)	Discharge (m^3/s)
			2/6/2014		651.29
			2/7/2014		339.80
	0.04	0.04	2/8/2014	0.1016	146.40
	0.01	0.01	2/9/2014	0.0254	170.47
			2/10/2014		212.09
			2/11/2014		237.86
			2/12/2014		229.93
			2/13/2014		222.85
	0.38	0.48	2/14/2014	1.0922	218.04
	0.04	0.2	2/15/2014	0.3048	228.52
			2/16/2014		224.27
	0.26	0.2	2/17/2014	0.5842	179.25
			2/18/2014		145.54
	0.1	0.13	2/19/2014	0.29	96.56
	0.21		2/20/2014	0.53	130.25
	0.13		2/21/2014	0.33	202.74
	0.04		2/22/2014	0.10	288.83
	0.02	0.06	2/23/2014	0.10	190.57
		0.06	2/24/2014	0.15	189.43
			2/25/2014		220.021
			2/26/2014		215.20
			2/27/2014		158.00
			2/28/2014		117.79
			3/1/2014		80.13
	1.2	1.43	3/2/2014	3.34	65.97
		0.21	3/3/2014	0.53	300.15
	0.03	0.31	3/4/2014	0.43	322.81
	0.41	0.49	3/5/2014	1.14	197.65
	0.25	0.33	3/6/2014	0.73	252.01
	0.07		3/7/2014	0.17	286.00
			3/8/2014		345.46
			3/9/2014		356.79
			3/10/2014		314.31
			3/11/2014		257.68
	0.07	0.07	3/12/2014	0.17	173.01
			3/13/2014		98.54
			3/14/2014		83.25

Knob Lick Precipitation (in)	Rex Precipitation (in)	Glasgow Airport Precipitation	Date	Average Precipitation (cm)	Discharge (m^3/s)
			3/15/2014		74.19
	0.24	0.33	3/16/2014	0.72	68.52
	0.02	0.01	3/17/2014	0.03	68.24
			3/18/2014		72.20
			3/19/2014		54.08
			3/20/2014		46.43
			3/21/2014		41.05
			3/22/2014		37.37
			3/23/2014		34.54
			3/24/2014		31.71
	0.01		3/25/2014	0.02	29.73
			3/26/2014		28.23
		0.24	3/27/2014	0.60	26.81
	0.26	0.02	3/28/2014	0.35	29.73
	0.46	0.22	3/29/2014	0.86	30.86
			3/30/2014		61.16
		0.01	3/31/2014	0.02	92.87
			4/1/2014		84.38
		0.36	4/2/2014	0.91	121.47
	2.12	0.93	4/3/2014	3.87	118.93
	0.39	0.49	4/4/2014	1.11	419.08
			4/5/2014		436.07
			4/6/2014		275.23
	0.25	0.19	4/7/2014	0.55	203.88
0.09	0.16	0.28	4/8/2014	0.44	178.11
	0.05	0.01	4/9/2014	0.07	161.68
			4/10/2014		149.79
			4/11/2014		156.30
			4/12/2014		170.46
			4/13/2014		146.96
	0.33	0.27	4/14/2014	0.76	113.55
	0.22	0.25	4/15/2014	0.59	99.95
			4/16/2014		80.41
			4/17/2014		63.14
			4/18/2014		56.06
			4/19/2014		43.32
			4/20/2014		33.98

Knob Lick Precipitation (in)	Rex Precipitation (in)	Glasgow Airport Precipitation	Date	Average Precipitation (cm)	Discharge (m^3/s)
			4/21/2014		30.29
0.03	0.09	0.02	4/22/2014	0.11	28.60
			4/23/2014		27.26
			4/24/2014		25.54
0.22	0.84	0.39	4/25/2014	1.22	25.59
			4/26/2014		43.60
	0.04	0.03	4/27/2014	0.08	37.66
	3.1	2.83	4/28/2014	7.53	45.59
2.52	0.23	0.1	4/29/2014	2.41	385.10
0.33	0.02	0.04	4/30/2014	0.33	481.38
0.04	0.02	0.18	5/1/2014	0.20	242.95
		0.6	5/2/2014	1.52	175.56
			5/3/2014		192.55
			5/4/2014		205.58
			5/5/2014		208.12
			5/6/2014		198.78
			5/7/2014		191.42
			5/8/2014		185.19
	0.44		5/9/2014	1.11	142.43
0.78	0.53		5/10/2014	1.66	58.61
0.23	0.01		5/11/2014	0.30	73.34
			5/12/2014		62.01
			5/13/2014		54.65
0.99	2.09	2.83	5/14/2014	5.00	81.55
2.55	0.02	0.02	5/15/2014	2.19	317.14
		0.06	5/16/2014	0.15	376.61
			5/17/2014		173.01
			5/18/2014		150.92
			5/19/2014		130.82
			5/20/2014		80.13
			5/21/2014		53.23
0.13	0.34	0.07	5/22/2014	0.45	46.43
0.07	0.1	0.09	5/23/2014	0.22	45.59
			5/24/2014		39.92
	0.02		5/25/2014	0.05	35.67
	0.1	0.21	5/26/2014	0.39	33.41
	0.01		5/27/2014	0.02	29.44

Knob Lick Precipitation (in)	Rex Precipitation (in)	Glasgow Airport Precipitation	Date	Average Precipitation (cm)	Discharge (m^3/s)
	0.03	0.01	5/28/2014	0.05	28.31
0.08	0.02		5/29/2014	0.12	28.20
			5/30/2014		31.99
			5/31/2014		28.26

APPENDIX G: FIELD NOTATION DELINEATED

Thesis Sample ID	Field Sample ID
S8 (0-2.5)	HC_BSC_0-1
S8 (2.5-7.5)	HC_BSC_1-3
S8 (7.5-15)	HC_BSC_3-6
S8 (15-25)	HC_BSC_6-10
S10 (0-2.5)	HC_BSC_HV_0-1
S10 (2.5-5)	HC_BSC_HV_1-2
S10 (5-10)	HC_BSC_HV_2-4
S10 (10-15)	HC_BSC_HV_4-6
S10 (15-20)	HC_BSC_HV_6-8
S4 (0-2.5) 1st Trip	HC_CF_0-1
S4 (2.5-5) 1st Trip	HC_CF_1-2
S4 (5-10) 1st Trip	HC_CF_2-4
S4 (10-15) 1st Trip	HC_CF_NBSD_4-6
S4 (15-20) 1st Trip	HC_CF_NBSD_6-8
S4 (20-25) 1st Trip	HC_CF_NBSD_8-10
Sb3 (0-2.5) 1st Trip	HC_SB_0415_0-1
Sb3 (2.5-5) 1st Trip	HC_SB_0415_1-2
Sb3 (5-10) 1st Trip	HC_SB_0415_2-4
Sb3 (10-15) 1st Trip	HC_SB_0415_4-6
Sb3 (10-15) 2nd Run	HC_SB_0415_4-6
Sb3 (15-20) 1st Trip	HC_SB_0415_6-8
Sb3 (20-25) 1st Trip	HC_SB_0415_8-11
Sb6 (0-1)	HRC_SD_BSRF_0-1_4-30-14
Sb9 (0-1) 2nd Trip	HRC_SD_SP_0-1_5-1-14
Sb2 (0-1) 2nd Trip	HRC-SD-BD
Sb5 (0-1)	HRC_SD_HWM_0-1cm_4-29-14
Sb5 (0-1) 2nd Run	HRC_HWM_0-1_4-29-14
Sb5 (0-1) Run incorrectly	HRC_HWM_0-1_4-29-14_138000
Sb7 (0-1)	HRC-CCS
Sb3 (0-1) 3rd Trip	HRC-DS-BW
Sb4 (0-1)	HRC-DS-Ledge
Sb2 (0-1) 3rd Trip	HRC-FB-0-1
Sb2 (0-1) 2nd Run	HB-FB-0-1
Sb8 (0-1)	HRC-KB-Soil
Sb8 (0-1) 2nd Run	KB2_0-1
Sb11 (0-1)	HRC_LWR

Thesis Sample ID	Field Sample ID
Sb9 (0-1, L) 3rd Trip	HRC-SR-L
Sb9 (0-1, W) 3rd Trip	HRC-SR-W
Sb10 (0-1, L)	HRC_WR_L
Sb10 (0-1, W)	HRC-WR-W
Sb1 (0-1, H1)	HRC-TH-1
Sb1 (0-1, H2)	HRC-TH-2
Sb1 (0-1, H3)	HRC-TH-3
Sb1 (0-1, H4)	HRC-TH-4
Sb1 (0-1, H5)	HRC_TH-5
Sb1 (0-1, H6_	HRC_TH_6
Sb1 (1-2, H6)	HRC-TH-6_1-2
Sb1 (2-3, H6)	HRC-TH-6
S2 (0-1)	HC-Soil-CI
S6 (0-1)	HC-Soil-HBW-0-1
S9 (0-1)	HC-Soil-HR
S5 (0-1)	HC=Soil-JT
S1 (0-1)	HC-Soil-OR-0-1
S4 (0-1) 3rd Trip	HC-Soil-SD
S7 (0-1)	HC-Soil-WW-0-1

VITA

Caroline Broderick achieved her Bachelors of Science in Geology from the College of Charleston in August, 2011. She spent August of 2011 until May 2013 working as a congressional aide in Washington, D.C. in the offices of Congressmen Jeff Landry and David Vitter. She spent the summer and fall of 2013; spring and summer of 2014 and summer 2015 as a geology intern for Kimbrell and Associates, LLC in Baton Rouge, LA.